

Advances in low-energy fission

Karl-Heinz Schmidt and Beatriz Jurado

CENBG, CNRS/IN2 P3, Chemin du Solarium B.P. 120, F-33175 Gradignan, France

ABSTRACT

Some of the main advances in experimental methods, experimental results and theoretical ideas of the last decades in the field of nuclear fission are discussed. New approaches extended the availability of fissioning systems for experimental studies on low-energy fission considerably and provided a full identification of all fission products in A and Z for the first time. The systematics of available data gives a more comprehensive view on the influence of shell effects and pairing correlations on the fission-fragment mass and nuclear-charge distributions. These data reveal that in asymmetric fission of the actinides the position of the heavy component in Z is approximately constant. Theoretical arguments for this unexpected finding are not yet available. The modelling of the fission process with dynamical models is still very difficult, since the most advanced models in nuclear physics that have been developed for stationary states are not readily applicable to the decay of a meta-stable state. Semi-empirical methods exploiting powerful theoretical ideas like (i) the separability of the influences of fragment shells and macroscopic influences of the compound nucleus, (ii) the properties of a quantum oscillator coupled to the heat bath of the other nuclear degrees of freedom for describing the fluctuations of normal collective modes, and (iii) an early freeze-out of collective motion to include dynamical effects seem to give a good description of the observed general trends and reach the precision needed for technical applications. The transformation of part of the fission Q value into intrinsic excitation energy along the fission process and the division between the fragments, following the laws of statistical mechanics, is essential for explaining the observed features of prompt-neutron emission and the even-odd effect in fission-fragment element yields. The capability of this new approach for calculating high-quality data that are relevant for nuclear technology like the yields and the energies of fission-fragments, prompt neutrons and gammas without specific adjustment to experimental data is demonstrated. The importance of nuclear fission as a laboratory for studying the dynamics of non-equilibrium processes in mesoscopic objects under the influence of residual interactions is stressed.

Contents

I.	Introduction	3
II.	General remarks	3
III.	Experimental methods	5
IV.	Fission channels	6
V.	Prompt-neutron yields	11
VI.	Even-odd effect in Z yields	16
VII.	Charge polarization	18
VIII.	Fragment kinetic energies	19
IX.	Energy release by prompt neutrons and gammas	21
X.	Summary	26
	Appendix	28
	References	

I. INTRODUCTION

Since the discovery of nuclear fission by Hahn and Straßmann in 1939 [1], the progress in the understanding of this dramatic nuclear re-organization process has not ceased being stimulated by new experimental findings. Although the gross explanation of nuclear fission on the basis of the liquid-drop model was provided very soon by Bohr and Wheeler [2], new observations permanently revealed a more and more detailed view on the complexity of nuclear fission and created new challenges for theory. Research on nuclear fission, in particular low-energy fission, where the influence of nuclear structure is strong, also yielded profit for the understanding of nuclear properties in general. The observation of asymmetric fission promoted the development of the nuclear shell model [3, 4]. The existence of shape isomers proved that shell effects persist at large deformations [5]. In the 1980's, a rather comprehensive understanding of the fission process had seemed to be reached, which is documented in the well-known text book of Wagemans [6]. Among the most important achievements were the development of the concept of fission channels [7] and the study of the even-odd effect in fission-fragment Z distributions [8, 9]. But new discoveries in the domain of nuclear fission are emerging continuously up to present times. The present contribution emphasizes some new theoretical ideas, which solve long-standing problems, and a few very recent findings, which represent new puzzles to theory.

II. GENERAL REMARKS

The discovery of fission revealed that the ground state of the heaviest nuclei is barely bound. An excitation energy in the order of a few percent of their total binding energy is sufficient to induce the disintegration into two pieces in a collective shape evolution that resembles the division of living cells, releasing a huge amount of energy of about 200 MeV, see figure 1. Thus, the energy content of nuclear fuel is about 10^8 times larger compared to fossil fuels like coal, mineral oil or natural gas, which explains the importance of nuclear technology. Figure 2 shows the binding energy per nucleon according to the liquid-drop model as a function of the nuclear mass. The binding energy per nucleon decreases for light nuclei due to the increasing surface energy, and it decreases for heavy nuclei due to the increasing Coulomb energy. Thus, energy is released in the fusion of light nuclei and in the fission of heavy nuclei. The energy stored in heavy nuclei, and even the synthesis of an appreciable portion of matter in the Universe has its origin in the r-process, a process of consecutive neutron capture and beta decay in an environment with a very high neutron flux in some astrophysical site, which is not yet fully identified [10].

Nuclear fission offers a rich laboratory for a broad variety of scientific research on nuclear properties, astrophysics and general physics. The r-process nucleosynthesis cannot be fully understood without a precise knowledge of the fission properties of very neutron-rich isotopes of the heaviest elements, which are presently not accessible to direct measurements [11]. The relatively flat potential energy reaching to very large deformations allows studying nuclear properties like shell effects in super- and hyper-deformed shapes [12]. Phenomena connected with the decay of the quasi-bound nuclear

system beyond the fission barrier yield information on nuclear transport properties like nuclear viscosity [13] and heat transfer between the nascent fragments [14]. They even offer a valuable test ground of general importance for non-equilibrium processes in mesoscopic systems, where quantum mechanics and microcanonical thermodynamics play an important role [15].

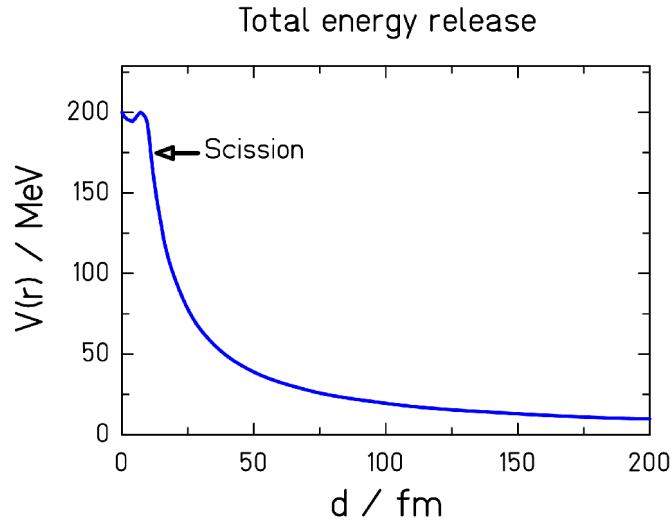


Figure 1. Potential energy released in the fission of ^{238}U as a function of the distance d between the centres of the fragments. Shell effects are neglected. In the mono-nuclear regime, d denotes the distance between the centres-of-mass of the two halves of the nucleus [16].

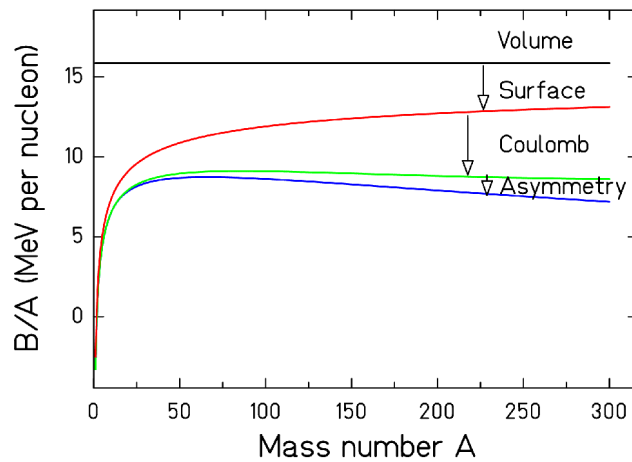


Figure 2. The different contributions to the binding energy per nucleon of nuclei along the beta-stability line according to the liquid-drop model [17]. The total binding energy per nucleon (lowest blue line) is maximum around $A = 56$. Lighter nuclei as well as heavier nuclei are less bound.

Even after more than 70 years of intense research, nuclear fission is still far from being fully understood. The present status in experimental knowledge and theoretical understanding is not yet satisfactory. There exist a number of valuable experimental signatures of fission like the mass and nuclear-charge division, the fragment kinetic energies as well as prompt neutron and gamma yields. However, overcoming present restrictions in the choice of fissioning systems and obtaining the necessary experimental resolution still requires a substantial technological effort. Also in the theory of fission, important progress has been achieved. The potential-energy surface of the fissioning systems has been systematically mapped in five-dimensional deformation space [18]. Stochastic methods [19, 20, 21, 22] and self-consistent microscopic approaches [23] have been developed for dynamical calculations of low-energy fission, however, still facing severe restrictions. The theoretical understanding of the fission process cannot fully rely on the powerful standard methods conceived for describing static nuclear properties; it requires developing new methods for modelling non-equilibrium processes in nuclei, e.g. [24, 25]. At present, combining available experimental information, e.g. [26, 27] with a large variety of long-standing and newly developed theoretical ideas proves to be the most successful approach for quantitative predictions to be used in nuclear technology and for considerable progress in understanding certain aspects of nuclear fission [28, 29].

III. EXPERIMENTAL METHODS

Available fissionable nuclei

The progress in the understanding of fission heavily relied and still relies on the development of advanced experimental methods. A severe restriction is still the availability of fissionable material as target material. Therefore, the traditional use of neutrons for inducing fission offers only a rather limited choice of fissioning systems. These limitations were more and more overcome by alternative methods: Spontaneously fissioning heavy nuclei were produced by fusion reactions [30]. Exotic nuclei were produced in spallation reactions which undergo beta-delayed fission [31]. Electromagnetic-induced fission of neutron-deficient radioactive nuclei, produced as projectile fragments from a ^{238}U primary beam, was studied in-flight at relativistic energies [32]. Very recently, comprehensive studies on fission of transfer products of ^{238}U projectiles have been performed [33, 34]. Very interesting experiments on fission of fragmentation products of ^{238}U relativistic projectiles induced by tagged photons will be possible with the ELISE electron-ion collider ring at the future FAIR facility [35].

Detection and resolution

The identification of fission products poses a severe problem. First experiments, which were based on radiochemical methods [36], were not fast enough to determine the yields of short-lived fragments and suffered from normalization problems. Kinematic identification methods by double time-of-flight [37, 38] and double-energy measurements [39] provided full mass distributions, however with limited resolution. The LOHENGRIN spectrograph brought big progress in fully identifying the *light* fission products in mass *and* nuclear charge [40]. However, full isotopic identification (in Z and A) of *all* fission products has only been achieved by boosting the energies of the products in inverse-kinematics experiments and using powerful magnetic spectrometers [32, 33, 41].

IV. FISSION-FRAGMENT YIELDS

Symmetric and asymmetric fission

Bohr and Wheeler [2] explained the phenomenon of nuclear fission by the influence of the Coulomb repulsion in heavy nuclei that favours elongated shapes and, finally, the separation onto two fragments of preferentially equal size. Figure 3 schematically shows the height of the barrier, which stabilizes the nucleus against fission, as a function of mass asymmetry. In light nuclei, the surface energy dominates, and the barrier for symmetric splits is maximum. In heavy nuclei, the Coulomb energy is decisive, and the barrier for symmetric splits is minimum. This transition occurs near $Z^2/A = 22$ [42, 43]. The fission-barrier height in ^{235}U is only about 5 MeV.

However, Bohr and Wheeler could not explain the predominant asymmetric mass division in the fission of the actinides. Maria Goeppert-Maier [3] traced the asymmetric fission back to nuclear shell effects, in particular to the stabilizing influence of the 50 proton shell and the 82 neutron shell that coincide in the spherical doubly magic ^{132}Sn . The existence of shell effects in deformed nuclei, which play an even more important role in nuclear fission, evidenced by the existence of shape isomers [44] and shell-stabilized strongly deformed fragments at scission [45], was introduced later by S. G. Nilsson [5].

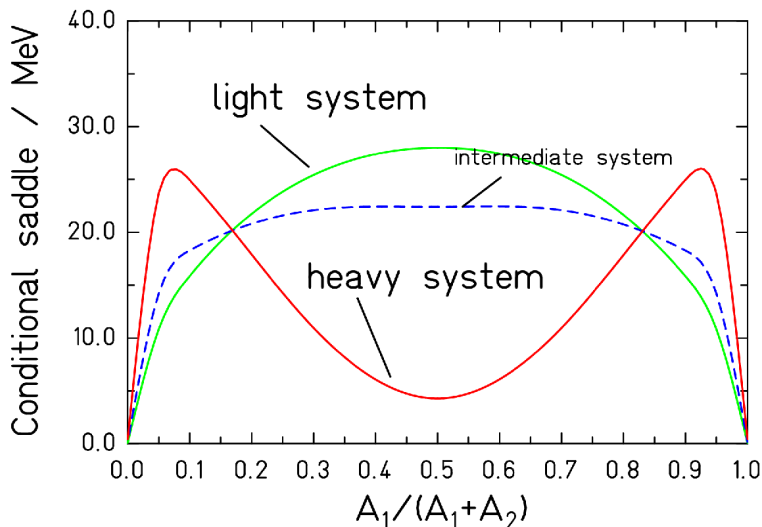


Figure 3. Schematic presentation of the fission-saddle height under the condition of a specific mass asymmetry according to the liquid-drop model.

Experimental systematics

Figure 4 gives an overview on the measured mass and nuclear-charge distributions of fission products from low-energy fission. Fission of target nuclei in the actinide region, mostly induced by neutrons, shows predominantly asymmetric mass splits. A transition to symmetric mass splits is seen around mass 258 in spontaneous fission of fusion residues.

Electromagnetic-induced fission of relativistic secondary beams covers the transition from asymmetric to symmetric fission around mass 226. A pronounced fine structure close to symmetry appears in ^{201}Tl [46] and in ^{180}Hg [31]. It is difficult to observe low-energy fission in this mass range. Thus, ^{201}Tl could only be measured down to 7.3 MeV above the fission barrier due to its low fissility, which explains the filling of the minimum between the two peaks. Only ^{180}Hg was measured at energies close to the barrier after beta decay of ^{180}Tl . Considering the measured energy dependence of the structure for ^{201}Tl [31], the fission characteristics of these two nuclei are rather similar. Also other nuclei in this mass region show similar features [47].

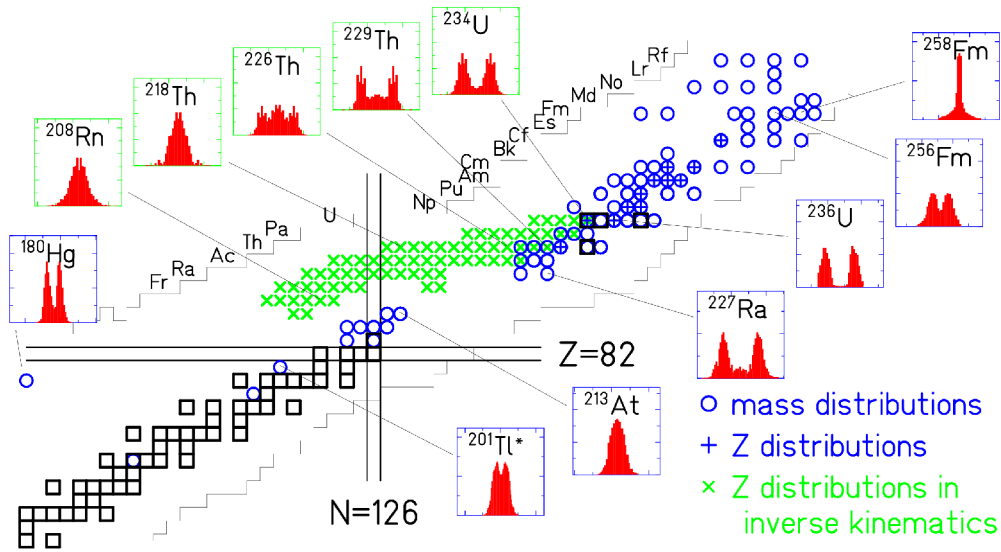


Figure 4. General view on the systems for which mass or nuclear-charge distributions have been measured. The distributions are shown for 12 selected systems. Blue circles (blue crosses): Mass (nuclear-charge) distributions, measured in conventional experiments [31, 46] and references given in [32]. Green crosses: Nuclear-charge distributions, measured in inverse kinematics [32].

Size of the heavy fragment in asymmetric fission

In the range where asymmetric fission prevails, e.g. from ^{227}Ra to ^{256}Fm , the light and the heavy fission-product components gradually approach each other with increasing mass of the fissioning nucleus, see figure 4. A quantitative analysis reveals that the mean mass of the heavy component stays approximately constant [48] at about $A=140$. This has been explained by the influence of a deformed ($\beta \approx 0.6$) fragment shell at $N=88$ and the spherical shell at $N=82$ [45], suggesting that the position of the heavy fragment is essentially constant in neutron number.

New data on Z distributions over long isotopic chains [32], however, reveal very clearly that the position in neutron number varies systematically over more than 7 units, while the position in proton number is approximately constant at $Z=54$, see figure 5. The rather

short isotopic sequences covered in former experiments did not show this feature clearly enough and gave the false impression of a constant position in mass.

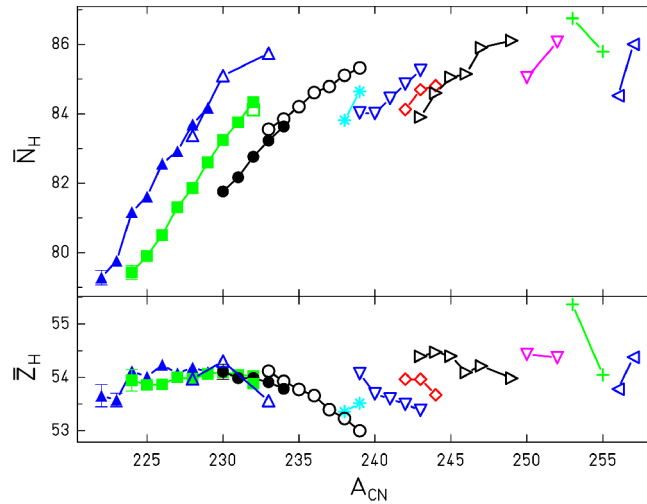


Figure 5. Mean neutron and proton number of the heavy component in asymmetric fission in the actinide region from thorium to einsteinium. The lines connect the data for a fixed element. The values were deduced from measured mass and nuclear-charge distributions using the semi-empirical GEF code [29] for the correction of charge polarization (the deviation of the N/Z ratio of the primary fragments before emission of prompt neutrons from the N/Z value of the fissioning nucleus) and prompt-neutron emission. Open symbols denote results from conventional experiments, full symbols refer to an experiment with relativistic projectile fragments of ^{238}U [28]. (See [29] for references of the underlying experimental data.)

This finding represents a severe puzzle to theory, since shell-model calculations do not show any shell stabilization near $Z=54$ at $\beta \approx 0.6$ [45, 49].

Separability principle

The microscopic-macroscopic approach has proven to be very useful for calculating nuclear properties, in particular in applications to fission [50]. The early influence of fragment shells on the fission path, deduced from two-centre shell-model calculations [51], makes its application to fission even more powerful. It means that the microscopic properties of the fission observables are essentially determined by the shells of the fragments, and only the macroscopic properties are specific to the fissioning system [52]. This “separability principle” was exploited in the GEF code [29], which relies on an empirical description of the macroscopic stiffness parameters for the relevant normal modes [61], which move perpendicular to the fission direction in collective-coordinate space, and empirically deduced fragment shells, which are valid for all fissioning systems.

The basic ideas of the GEF code follow closely the statistical approach introduced by Jensen and Døssing [53] where the mass distribution in fission is given by the available number of states above the potential-energy surface. However, GEF includes a few important modifications: (i) The shell effects that were calculated from single-particle energy spectra in a Woods-Saxon potential with the Strutinsky method in ref. [53] are replaced by global fragment shells, which are adjusted to the measured mass distributions. The separability principle simplifies this task considerably, since the fragment shells are assumed to depend only on the fragment, and, thus, they are the same for all fissioning systems. (ii) The nuclear level density that was calculated from the same single-particle spectrum including pairing correlations using the BCS approximation in ref. [53] is replaced by an empirical constant-temperature formula [54], which seems to be in better agreement with recent experimental results [55]. In addition, the shapes of the fragments at scission, the charge polarization, the angular momenta, and other properties of the fragments as well as the emission of prompt neutrons and gamma rays are calculated on the basis of similar ideas. See ref. [29] for a detailed description of the code. In figure 6, some experimental mass and nuclear-charge distributions are compared with the results of the GEF code. The data over a large range of systems can be described very well with the same parameter set. The most important parameters are the positions, the depths and the widths of 3 fragment shells for the standard 1, the standard 2 and the super-asymmetric fission channel [7], which are described with the same 14 parameter values for all systems. The narrow symmetric fission in the heaviest nuclei results from the superposition of the standard-1 shells in the two fragments and, thus, does not require any additional parameter.

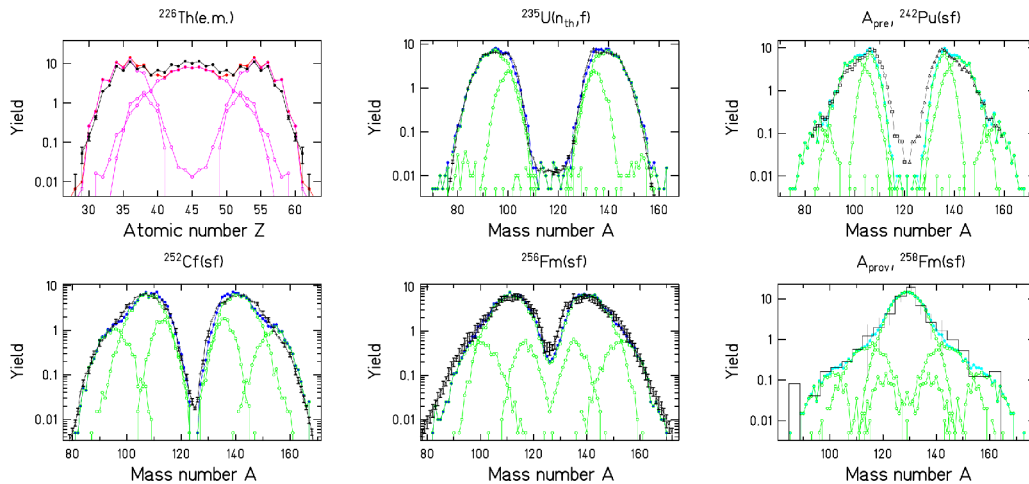


Figure 6. Mass and Z distributions of fission fragments from spontaneous fission (sf), thermal-neutron-induced fission (nth,f) and electromagnetic-induced fission (e.m.). (In most cases the post-neutron masses are shown. A_{prev} is the “provisional mass” that is directly deduced from the ratio of the kinetic energies of the fragments and, thus, it is not corrected for neutron emission.) Measured or evaluated data (black lines, respectively histogram) are compared with predictions of the GEF code [29] (pink and green lines). The contributions of different fission channels are shown. (See [29] for references of the data.)

A comprehensive overview on almost all available mass distributions is given in the appendix. The general good agreement between the GEF calculations and the data shows that the complex variation of the mass distributions of the different fissioning systems has a rather simple origin on the basis of the concept of fission valleys formed by the shell effects, superimposed on the macroscopic global potential-energy surface. Some of the discrepancies are probably caused by shortcomings of the evaluated files due to insufficient experimental information, e.g. for $^{229}\text{Th}(n_{\text{th}},f)$ and $^{255}\text{Fm}(n_{\text{th}},f)$.

Dynamical effects

Statistical scission-point models, e.g. ref. [45], suffer from the neglect of dynamical effects. Stochastic calculations revealed that, depending on the nature of the collective degree of freedom, dynamical effects induce a kind of memory on the fission trajectory, which may be accounted for by assuming an early freeze-out that depends on the influence of inertia. Mass-asymmetric distortions have a large inertia, and, thus, the mass distribution is already essentially determined slightly behind the outer fission saddle [56]. This has been confirmed by experimental mass distributions whose widths are in agreement with the assumption that they are determined by the stiffness of the potential near saddle, which is smaller than the stiffness of the potential at scission [48]. In the GEF code, the underlying macroscopic potential is deduced from the measured mass distributions [57]. Thus, it effectively includes dynamical effects. Charge polarization has a small inertia, and the distribution is determined close to scission [58]. Other quantities that change during the descent from saddle to scission, e.g. the intrinsic excitation energy, have less effect on the fission observables, since the normal modes are hardly excited, see next section.

Quantum-mechanical effects

Most fission observables form bell-shaped distributions around a mean value. This suggests treating the corresponding collective degree of freedom as an harmonic quantum oscillator coupled to a heat bath of temperature T with limited excitation energy. Especially for the charge-polarization degree of freedom there exists a long discussion about the importance of the zero-point motion [59, 60], which implies that at zero excitation energy the variance of the probability distribution is given by $\frac{\hbar}{2C}$, where $\hbar\omega$ is the energy difference between the harmonic-oscillator states and C is the stiffness of the parabolic potential. Nix estimated the level spacing $\hbar\omega$ in the oscillator corresponding to mass-asymmetric distortions at saddle with the liquid-drop model to 1-2 MeV in the actinide region [61]. According to the smaller widths of the corresponding components of the mass distribution, the level spacing for oscillations in the two asymmetric fission valleys (standard 2 and standard 1) is about 5 and more than 10 MeV, respectively. Also for oscillations in the charge-polarization degree of freedom, the level spacing is in the order of 10 MeV. These values are appreciably larger than the temperature values of actinides, which are about 0.5 MeV in the constant-temperature regime [54]. Thus, in a statistical approach these degrees of freedom are essentially not

excited, and the widths of the corresponding distributions are essentially determined by the zero-point motion.

Also the angular-momentum distributions of the fragments have been explained by “orientation pumping” due to the uncertainty principle [62]. Experimental indications for thermal excitations of spherical fragments [63] have also been explained by the compensation of the orbital angular momentum, which itself is induced by the zero-point motion [64]. Here, it is the operator of the orbital angular momentum which does not commute with the angle that characterizes the direction of particle motion. Thus, all fragment angular momenta measured in low-energy fission are explained by the quantum-mechanical uncertainty principle. There is no room for excitations of the angular-momentum-bearing modes [65].

Due to the strong influence of quantum-mechanical effects it is mandatory to explicitly consider these, as it is e.g. done in the self-consistent microscopic approach of ref. [23]. Stochastic approaches with classical models, e.g. ref. [21] seem to be inadequate. In the GEF code, the influence of the zero-point motion on the different observables is considered by calculating the probability distribution in the quantum oscillator [66] corresponding to the respective normal mode [61] as a function of nuclear temperature and excitation energy.

V. PROMPT-NEUTRON YIELDS

Transformation of energy – the different contributions

In low-energy fission, the available energy, consisting of the Q value of the reaction plus the initial excitation energy of the fissioning nucleus, ends up either in the total kinetic energy (TKE) or the total excitation energy (TXE) of the fragments, since particle emission before scission may be neglected. The TKE is closely related to the distance of the centres of the two nascent fragments at scission, but it cannot give information on the shapes of the individual fragments. The TXE, however, can be attributed to the individual fragments by a kinematical measurement of the prompt neutrons. Still, there is no direct experimental information on the processes, which are responsible for the transformation of part of the available energy into the excitation energies of the separated fragments. The situation is schematically illustrated in figure 7. Before scission, dissipation leads to intrinsic excitations. In addition, collective modes perpendicular to the fission direction (normal modes [61]) may be excited, and, finally, some energy is stored in deformation of the nascent fragments that is induced by the Coulomb repulsion. At scission, this energy still appears as part of the potential energy in figure 7. The remaining part is found as pre-scission kinetic energy [67]. Well after scission, collective excitations and deformation energy are transformed and add up to the intrinsic excitations of the separated fragments.

The situation at scission is important for the understanding of fission dynamics, e.g. the magnitude of dissipation and the coupling between the different collective degrees of freedom, but without additional information the energy repartition remains ambiguous.

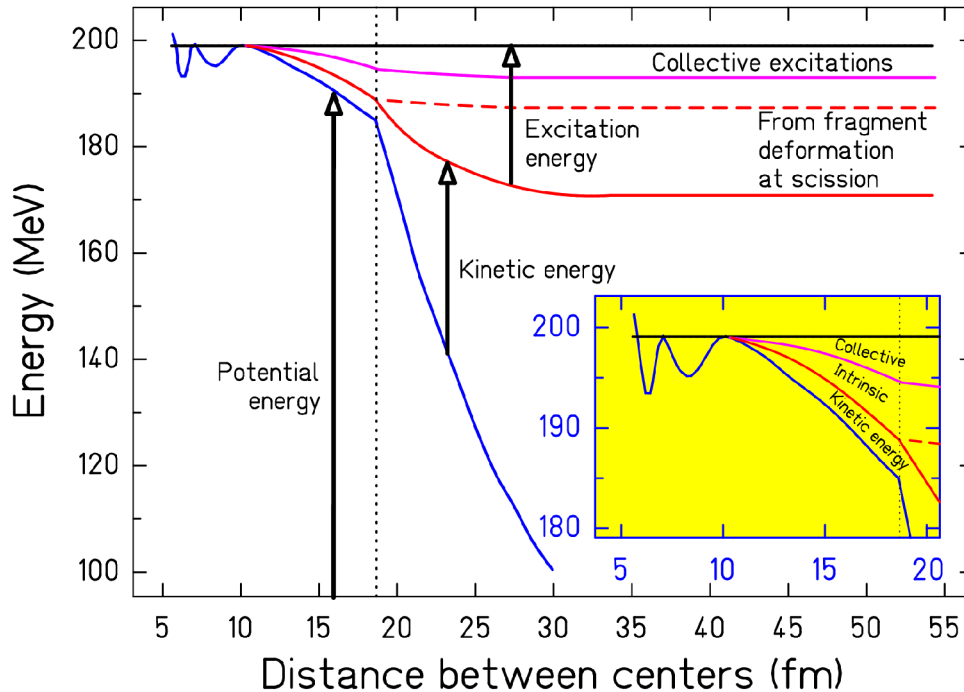


Figure 7. Schematic drawing of the transformation of energy during the fission process of ^{236}U with an initial excitation energy equal to the height of the fission barrier. The vertical dotted line indicates the scission point, and the inset represents a zoom of the situation at scission. (Adapted from figs. 7 to 9 of ref. [68].)

Origin of the saw-tooth shape

There is widespread agreement that the saw-tooth shape of the prompt-neutron yields, see figure 8, is caused by the deformation energies of the nascent fragments at scission. The scission-point model of ref. [45] attributes the dips around $A=130$ to the influence of spherical fragment shells. The random-neck-rupture model [7] links the saw-tooth shape to the location of the rupture. The number of emitted neutrons increases with the surface of the neck, and also microscopic calculations predict large deformation energies of the fragments near scission [69]. Large even-odd effects in the fragment Z distributions indicate that the probability for populating the fragments in their ground state is rather high, see the dedicated discussion below. Thus, the intrinsic excitation energy at scission is generally much too low to account for the variation of the prompt-neutron yield by several units over the different fragments.

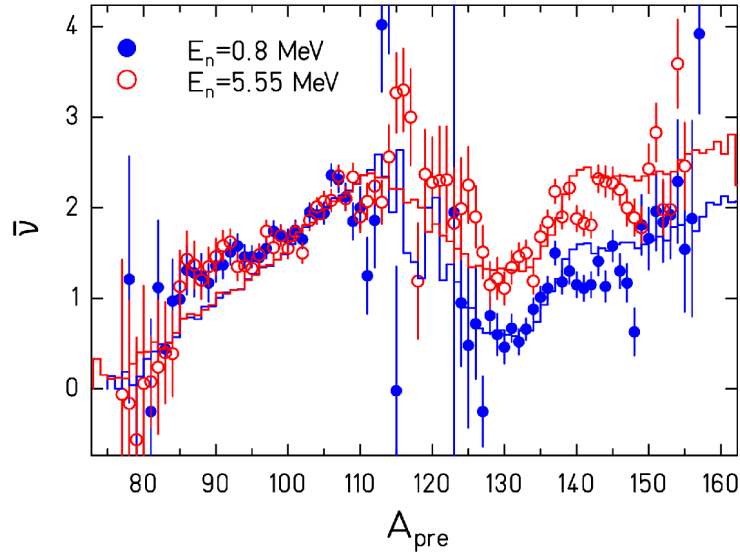


Figure 8. Measured prompt-neutron yield in $^{237}\text{Np}(n,f)$ as a function of pre-neutron mass at two different incident-neutron energies [70] (data points) in comparison with the result of the GEF code [29] (histograms).

Energy dependence of neutron yields – energy sorting

Recent experimental results indicate that nuclei exhibit an essentially constant temperature T up to excitation energies of 20 MeV [55]. According to empirical systematics, the temperature parameter T is grossly proportional to $A^{-2/3}$ [54]. The temperature is deduced from the energy-dependent nuclear state density $\omega(E)$, or approximately from the energy-dependent nuclear level density $\rho(E)$ [71] and is defined as $T = (d \ln \omega / d E)^{-1} \approx (d \ln \rho / d E)^{-1}$. The constant-temperature behaviour is explained by the breaking of pairs in the so-called superfluid regime [72]. This leads to a considerable increase of the heat capacity $C = dE/dT$ [73] and consequently to a slow variation of temperature T as a function of excitation energy E . Thus, the assumption of a constant nuclear temperature T becomes a good approximation. Note that the BCS approximation severely underestimates the pairing condensation energy E_{cond} and consequently also the magnitude of the heat capacity in the so-called superfluid regime [74]. Thus, the constant-temperature description might be approximately valid up to higher energies than usually considered.

The configuration before scission consists of two nuclei being in thermal contact by the neck. The two nuclei may be considered as two heat baths with different energy-independent temperatures, T_1 and T_2 , and a constant amount of total intrinsic excitation energy (see the inset in figure 7) $E = E_1 + E_2$ to be shared. A rough estimation of the thermodynamical properties of this system may be deduced from the entropy as a function of energy division:

$$S = S_1 + S_2 = \frac{E_1}{T_1} + \frac{E_2}{T_2} = \frac{E_1}{T_1} + \frac{E - E_1}{T_2} = \frac{T_1 E + (T_2 - T_1) \cdot E_1}{T_1 \cdot T_2} \quad (1)$$

Figure 9 shows a numerical example. Since there exists no equilibrium solution with $T_1 = T_2$, one can only argue that the system develops in the direction of increasing entropy. This implies that the intrinsic excitation energy of the two nascent fragments at scission is subject to energy sorting [14, 75, 76]: The hotter light fragment transfers essentially all its intrinsic excitation energy to the colder heavy fragment.

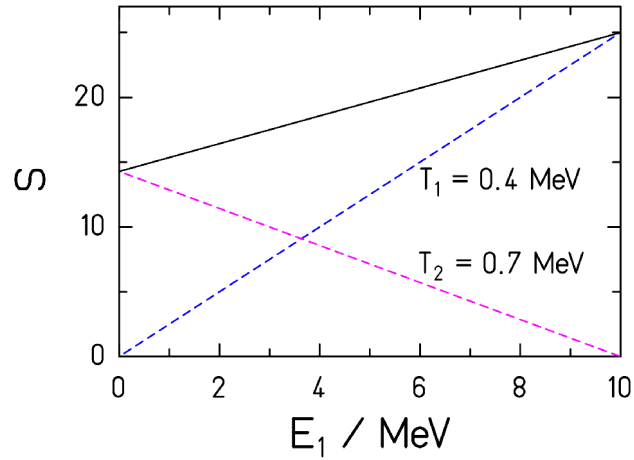


Figure 9. Entropy of the pre-scission configuration as a function of energy division. The temperatures of the two nascent fragments are assumed to be 0.4 MeV and 0.7 MeV and the total intrinsic excitation energy is $E = E_1 + E_2 = 10$ MeV. The dashed lines represent the entropy of the individual fragments $(E_1)/T_1$ and $(E - E_1)/T_2$. The full line is the total entropy of the system made of two fission fragments in contact.

A more realistic estimation of the problem is illustrated in figure 10. From a microscopic point of view, the exchange of excitation energy between the nascent fragments may be performed by the exchange of nucleons across the neck. The different single-particle occupation functions, corresponding to the different temperatures, cause an enhanced transfer of particles from the heavy to the light fragment below the Fermi surface and an enhanced transfer of particles from the light to the heavy fragment above the Fermi surface, as illustrated in figure 10. Both processes lead to a transport of excitation energy from the light to the heavy fragment.

This energy transport may be considered as a kind of second-order window formula. While the window formula of the one-body dissipation [77] leads to energy dissipation, that means heating of both reaction partners, due to the relative velocity of the reaction partners, the energy sorting in fission is caused by the different slopes of the single-particle occupation functions. Fission provides a rather unique scenario for the phenomenon of energy sorting between nuclei, because the relative velocity of the

nascent fragments before fission is very small compared to the Fermi velocity, and thus the heating due to one-body dissipation is small. This is not the case in most nuclear reactions.

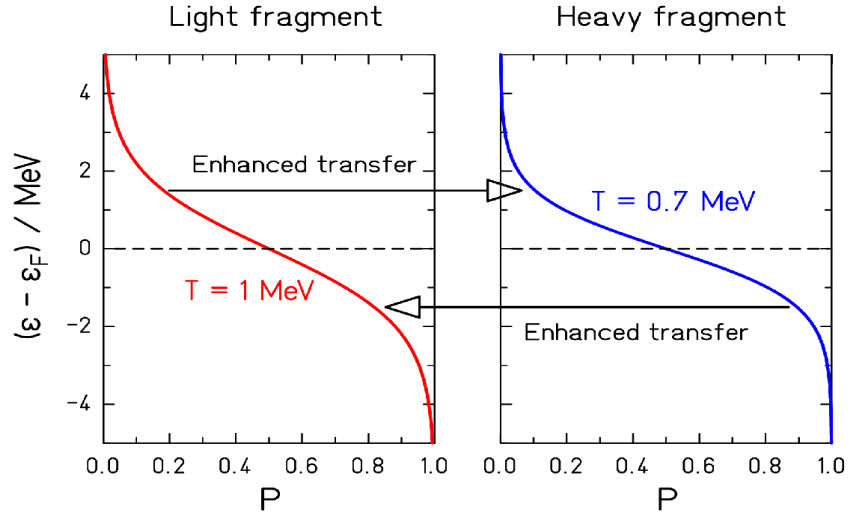


Figure 10. Single-particle occupation probabilities of the two nascent fragments in the pre-scission configuration.

This mechanism of energy transport aims to establish statistical equilibrium, which is given by the condition that all nuclear states, approximated by the nuclear level density ρ , are populated with the same probability:

$$\bar{E}_1 = \frac{\int_0^E E_1 \rho_1(E_1) \rho_2(E - E_1) dE_1}{\int_0^E \rho_1(E_1) \rho_2(E - E_1) dE_1} \quad (2)$$

The result of applying eq. (2) is shown in figure 11 for a specific example. Obviously, the energy sorting is not complete: The light fragment keeps an excitation energy of about 2 MeV. This is a kind of border effect, because there are no levels below the nuclear ground state. However, above 4 MeV there is a clear saturation of excitation energy in the light fragment, and any additional initial excitation energy is accumulated in the heavy fragment.

This energy sorting manifests itself in the mass-dependent neutron yields. Figure 8 shows data for neutron-induced fission of ^{237}Np with $E_n = 0.8$ MeV and $E_n = 5.55$ MeV [70] as an example. The additional initial energy leads to an increased neutron yield from the heavy fragments, only. This phenomenon can only be explained by the energy sorting mechanism. Indeed, an energy partition according to the mass ratio of the fragments, as it

is often assumed, would lead to an increase of the excitation energy in both fragments and thus to an increase of the number of prompt neutrons emitted by the light fragment also (see Figure 11). The behaviour is well reproduced by the GEF code, which includes a model for the process of energy sorting. The concentration of an increased initial excitation energy on the heavy fragment has also been found in neutron-induced fission of ^{235}U [78] at somewhat higher excitation energies in proton-induced fission [79].

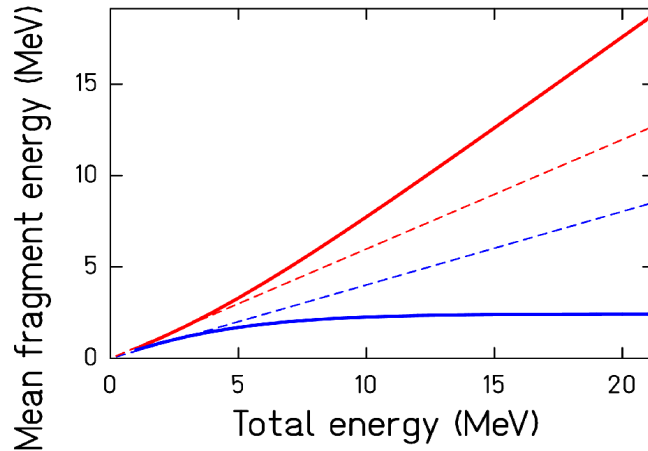


Figure 11. Mean energy division according to statistical equilibrium (eq. (2)) between the nascent fragments ^{94}Sr (lower blue full line) and ^{140}Xe (upper red full line) formed in $^{233}\text{U}(n,f)$. For comparison, the energy division according to the mass ratio is shown (dashed lines).

VI. EVEN-ODD EFFECT IN Z YIELDS

Experimental systematics

The production of fragments with even Z is generally enhanced in low-energy fission. Figure 12 shows the Z distribution measured in electromagnetic-induced fission of ^{226}Th . In this nucleus, the symmetric fission channel is rather strong, see figure 4, and thus the even-odd effect could be measured over the whole fission-fragment range. This observation solved the long-standing question, whether there is an even-odd effect in the symmetric fission channel, since the yield at symmetry of systems accessible by thermal-neutron-induced fission is very low [80].

A systematic view on the local even-odd effect [81] in fission-fragment Z distributions [82] reveals a regular pattern and a general dependence on the fissioning system, see figure 13. The magnitude of the even-odd effect is small at symmetry, and it increases strongly with increasing asymmetry. At the same time, the even-odd effect generally decreases for heavier systems. The even-odd effect in the light fragment group of even- Z and odd- Z systems is essentially identical. When approaching symmetry, the even-odd effect in even- Z systems is described by the superfluid nuclear model [83], while it goes to exactly

zero in odd- Z systems. Electromagnetic excitations lead to slightly higher excitation energies, thus reducing the magnitude of the even-odd effect. The large number of systems investigated [32] revealed that the appearance of a large even-odd effect at large asymmetry is a general phenomenon, also in odd- Z fissioning systems [84]. In every case, there is an enhancement for even- Z fragments in the light fragment group, indicating that it is the enhanced production of even- Z light fragments, which is at the origin of the large even-odd effect at extreme asymmetry. Since the quasi-particle excitations are expected to wash out any even-odd staggering in the nuclear excited states (see e.g. figure 9 in [84]), the enhanced production of even- Z fragments must essentially be attributed to the population of their fully paired “ground state” at scission.

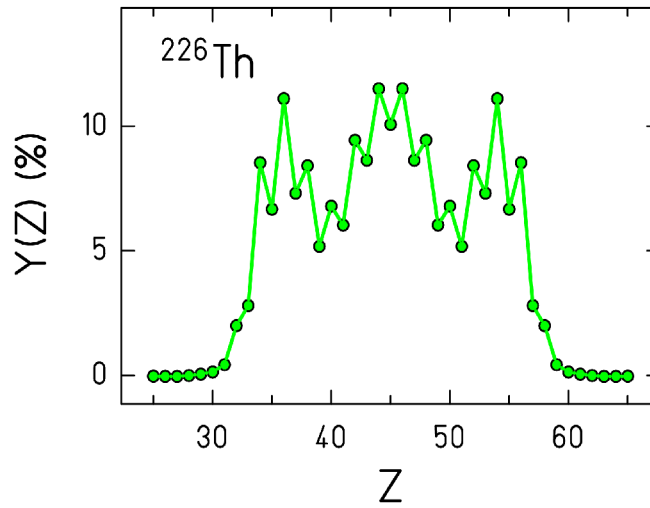


Figure 12: Fission-fragment element distribution measured in electromagnetic-induced fission of ^{226}Th [32].

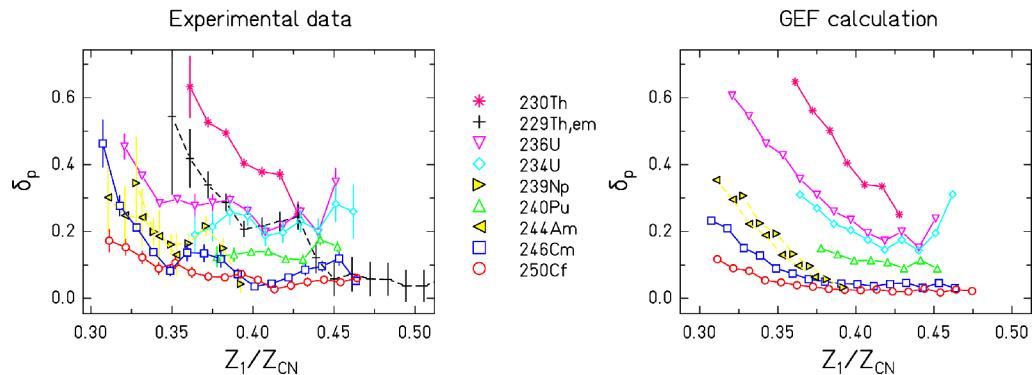


Figure 13. Measured (left) and calculated (right) local even-odd effect in fission-fragment Z distributions in (n_{th},f) reactions. The fissioning nuclei are indicated. Data for fission of ^{229}Th , induced by electromagnetic excitations are included. See ref. [82] for references of the data.

Final stage of energy sorting

It seems straightforward to attribute the enhanced production of even- Z light fragments to the energy-sorting mechanism [85] that explained already the differential behaviour of the prompt-neutron yields. If the time until scission is sufficient for the energy sorting to be accomplished, the system can still gain an additional amount of entropy by predominantly producing even-even light fragments. Compared to the production of odd-odd light fragments, the excitation energy of the heavy fragment increases by two times the pairing gap, and its entropy increases due to the increasing number of available states. The right part of figure 13 shows a calculation with the GEF code, where this idea is included in a schematic way. The basic features are: (i) The excitation energy induced by dissipation grows with the Coulomb parameter $Z^2/A^{1/3}$, and the time needed for complete energy sorting is correspondingly increased. This explains the observed reduction of the even-odd effect for heavier systems. (ii) The thermal pressure grows with increasing asymmetry, which accelerates the energy-sorting process. This explains the strong increase of the even-odd effect at large asymmetry.

The asymmetry-driven even-odd effect is thus a threshold phenomena, which sets in when the time needed for reaching the scission configuration, or more correctly speaking a configuration with a sufficiently high potential barrier between the nascent fragments to inhibit the transfer of protons, is sufficiently long for complete energy sorting. Fluctuations in the energy-sorting process are responsible for the smooth onset of the even-odd effect with increasing asymmetry.

VII. CHARGE POLARIZATION

Experimental information

The fission fragments are not fully specified by their mass number. While the total numbers of protons and neutrons of the two fission fragments at scission, i.e. before prompt-neutron emission, are given by the fissioning nucleus, the N/Z ratios of the fragments may be different. One fragment may be more, the other one less neutron-rich. This “charge polarization“ is essentially characterized by its mean value and its width.

Most experimental information on charge polarization at scission is indirect, because only the fragment masses after the emission of prompt neutrons can be measured with good resolution. Thus, the influence of prompt-neutron emission has to be corrected. This correction introduces some uncertainties, because most data on mass-dependent prompt-neutron multiplicities are not very precise, and for many systems such data are not available.

Figure 14 shows the measured deviation of the mean nuclear charge from the UCD (unchanged-charge-distribution) value for a fixed post-neutron mass and the standard deviation of the corresponding nuclear-charge distribution for the thermal-neutron-induced fission of ^{235}U [86]. The influence of the even-odd staggering of the Z yields is clearly visible in both quantities.

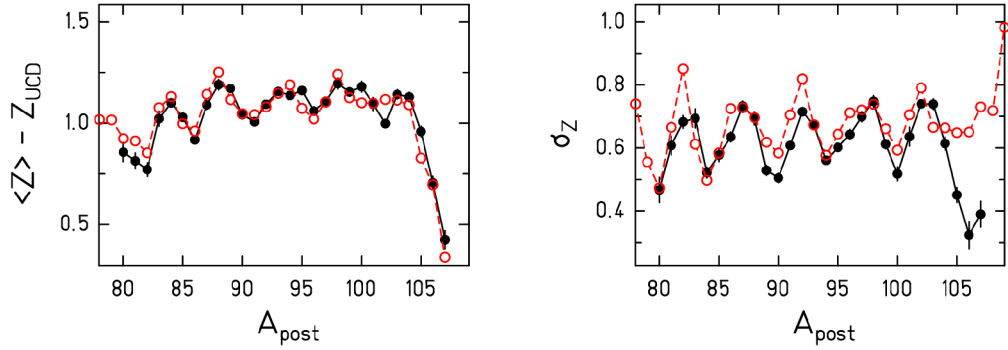


Figure 14. Indirect information on the charge polarization in $^{235}\text{U}(n_{th},f)$. Left part: Deviation of the mean nuclear charge from the UCD (unchanged charge distribution) value for a fixed post-neutron mass A_{post} . Experimental data [86] (full points) are compared with the result of the GEF code [29] (open points). Right part: Standard deviation of the nuclear-charge distribution for a fixed post-neutron mass A_{post} . Experimental data [86] (full points) are compared with the result of the GEF code [29] (open points).

Simulation

The simulation of the nuclear-charge distributions for fixed post-neutron mass starts from the calculated pre-neutron nuclide distribution and the excitation energy of each individual fragment. The emission of prompt neutrons must be considered, which is constrained by measured mass-dependent prompt-neutron-multiplicity distributions. The good agreement with post-neutron fragment distributions shown in figure 14 was obtained by minimizing the macroscopic potential energy of the scission configuration, approximated by quadrupole-deformed fragments with a tip distance of 3 fm, with respect to their N/Z ratios. However, for the asymmetric fission channels, the value of $\langle Z \rangle - Z_{UCD}$ had to be increased (decreased) by 0.3 units in the light (heavy) fragment. The mean deformation of the fragments at scission is linked to the mean prompt-neutron multiplicity, considering the amount of intrinsic excitation energy at scission, which is consistent with the description of the even-odd effect in the Z distributions.

It seems that shell effects are not only responsible for the asymmetry in the fission-fragment mass distribution, but they also tend to enhance the N/Z in the heavy fragment. This effect is expected for the standard 1 fission channel which is associated with the shell stabilization around the spherical doubly magic ^{132}Sn that is more neutron rich than most fissioning systems, but it seems that it is also present for the standard 2 fission channel which is characterized by strongly deformed heavy fragments. This problem has been addressed already in 1966 by Nörenberg [87], but, to our knowledge, it is not considered in modern microscopic theories.

VIII. FRAGMENT KINETIC ENERGIES

The fragment kinetic energy is a key quantity for the energetics of the fission process. Its magnitude has been exploited to extract information on the dissipation during the descent

from saddle to scission [88,20]. With the knowledge of the nuclide distribution of the primary fragments it defines the amount of excitation energy of the fragments, which feeds the emission of prompt neutrons and protons. The pre-scission kinetic energy competes with the intrinsic excitation energy at scission and is thus linked with the even-odd effect in fission-fragment yields, see discussion below. This demonstrates the complex interconnections of the different fission observables.

In the GEF code, the total kinetic energy of the fission fragments is given by subtracting the total excitation energy of the separated fragments from the sum of the initial excitation energy of the fissioning nucleus and the Q value of the fission process. Best agreement with all observables was obtained by assuming that 30% of the energy release from saddle to scission [89] is dissipated into intrinsic excitations. This may be compared with microscopic estimations [90]. The resulting distribution for $^{235}\text{U}(n_{\text{th}},f)$ is shown in figure 15. The overall behaviour is in agreement with expectations from systematics. In the model, the shape of the energy distribution for a fixed mass is mainly defined by the distribution of fragment deformations at scission, which is taken as a Gaussian distribution with a maximum in the respective potential minimum and a standard deviation of $\sigma_{\beta}=0.165$. These shapes define the amount of deformation energy of the separated fragments with respect to their respective ground state, which finally adds up to their intrinsic excitation energy. The kinetic energies obtained with this approach are rather realistic. Also the experimentally observed steeper slope on the high-energy side is reproduced, although the skewness seems to be slightly larger than found in experiment.

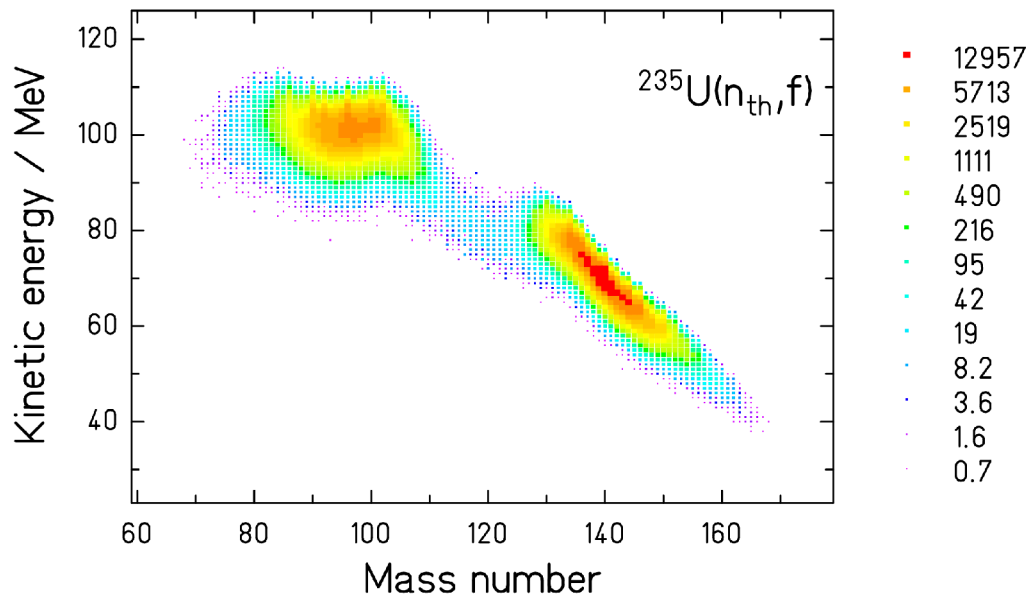


Figure 15. GEF calculation for the two-dimensional distribution of kinetic energies and fission-fragment masses before emission of prompt neutrons for $^{235}\text{U}(n_{\text{th}},f)$. The colour scale refers to the number of events in the Monte-Carlo calculation.

IX. ENERGY RELEASE BY PROMPT NEUTRONS AND GAMMAS

Importance for nuclear technology

The scientific interest in nuclear fission has seen a considerable revival during the last years. Great part of the motivation stems from the importance of nuclear fission for nuclear technology and, in particular, for the need of an extended data base for the planning of new-generation nuclear power plants. In the past, nuclear data with sufficient precision could only be obtained by dedicated experiments or direct adjustments of evaluations or empirical and semi-empirical models to experimental data. The "point-by-point model" [⁹¹, ⁹²] that provides detailed information on prompt-neutron and prompt-gamma emission is a prominent case of this kind of approach. It is based on the measured A-TKE distribution and, eventually, on the mass-dependent mean prompt-neutron multiplicities [⁹³] of the system considered. In many cases, this method is not applicable, because the required data are not available. Thus, there is great interest in a model with good precision and a predictive power for systems for which no experimental data exist. It is expected that the improved understanding of the fission process that is behind the model implemented in the GEF code helps to solve this problem, because it relies on a universal basis for all systems. This basis can be constructed from the systematics of the data of many fissioning systems and applied to any system, even if there are no experimental data available for a specific case.

The following sections show some applications of the GEF code for the predictions of prompt-neutron and prompt-gamma emission in fission. Both provide a considerable contribution to the heat production in the nuclear-fission process, which explains the importance of these data for nuclear technology.

Prompt-neutron multiplicities

Besides the mass-dependent mean prompt-neutron yields, see figure 8, there exist two other experimental results, which have been determined with high accuracy: The mean number of prompt fission neutrons and, in some cases, the mass-integrated neutron-multiplicity distribution.

The measured mean number of prompt-fission neutrons is compared in table 1 with the values given by the GEF code for some selected systems. The same parameter set was used for all systems. However, the TXE had to be increased by 1.6 MeV, equally shared between the fragments, for odd-*Z* fissioning systems, just as an empirical parameterisation. This is a general effect, found on the average over the whole range of fissioning systems. In contrast, there is no even-odd fluctuation in the neutron number of the fissioning nucleus. This is another unexpected and rather intriguing finding, for which we have no explanation.

Table 1. Mean prompt-neutron multiplicities for some selected systems. The measured values are compared with the result of the GEF code.

System	E_n	Exp.	GEF
²³⁵ U(n,f)	thermal	2.41 [⁹⁴]	2.40
²³⁵ U(n,f)	0.5 MeV	2.46 [78]	2.50

$^{235}\text{U}(n,f)$	5.55 MeV	3.19 [78]	3.28
$^{237}\text{Np}(n,f)$	0.8 MeV	2.73 [70]	2.80
$^{237}\text{Np}(n,f)$	5.55 MeV	3.46 [70]	3.53
$^{239}\text{Pu}(n,f)$	thermal	2.88 [94]	3.05
$^{252}\text{Cf}(sf)$	---	3.77 [95]	3.65

Figure 16 demonstrates the good agreement of the calculated neutron-multiplicity distributions for $^{235}\text{U}(n_{\text{th}},f)$ and $^{239}\text{Pu}(n_{\text{th}},f)$ with the experimental data. Like in the case of the fragment kinetic energies, the width is mostly caused by the distribution of fragment deformations at scission. The shape of the distribution is well reproduced for both systems.

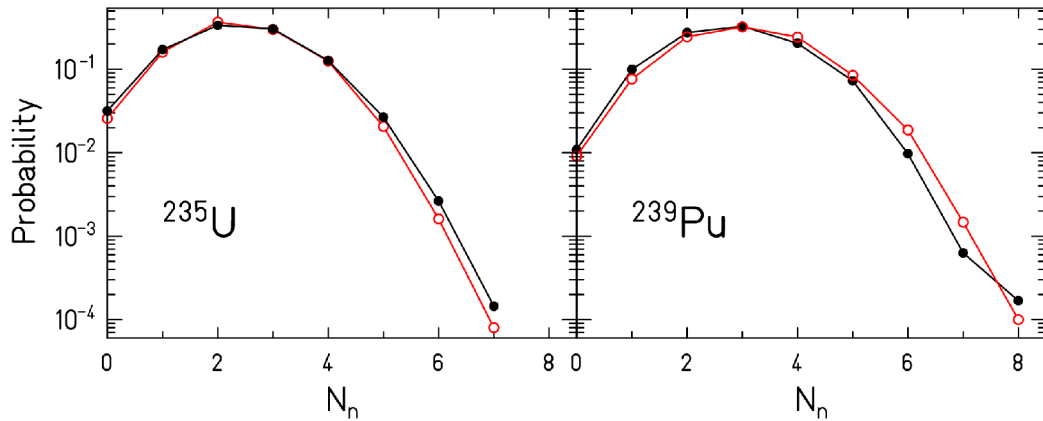


Figure 16. Measured prompt-neutron-multiplicity distributions [94] for $^{235}\text{U}(n_{\text{th}},f)$ (left part) and $^{239}\text{Pu}(n_{\text{th}},f)$ (right part) are compared to the results of the GEF code.

Prompt-neutron spectrum

The experimental prompt-fission-neutron spectrum for the system $^{235}\text{U}(n_{\text{th}},f)$ of ref. [102] is compared with the result of the GEF code in figure 17. In order to better visualize the slight deviations, figure 18 shows this comparison in a reduced presentation with both spectra normalized to a Maxwellian distribution with the parameter $T = 1.32$ MeV.

In this calculation, the de-excitation of the separated fragments has been obtained within the statistical model. It is assumed that both the emission of neutrons and the emission of E1 gammas does not change the angular momentum on the average, which seems to be a good approximation in the relevant angular-momentum range [96]. When the yrast line is reached, the angular momentum is carried away by a cascade of E2 gammas. Inverse total neutron cross sections with the optical-model parameters of ref. [97] were used. Gamma competition at energies above the neutron separation energy was considered. The gamma strength of the giant dipole resonance (GDR) following the description proposed in ref. [98] was applied. The nuclear level density was modelled by the constant-temperature description of v. Egidy and Bucurescu [99] at low energies. A good reproduction of the prompt-neutron spectrum suggests a slight reduction of the temperature value by 15%.

The level density was smoothly joined with the modified Fermi-gas description of Ignatyuk et al. [¹⁰⁰, ¹⁰¹] for the nuclear-state density:

$${}^{235}\text{U}(n_{\text{th}}, f)$$

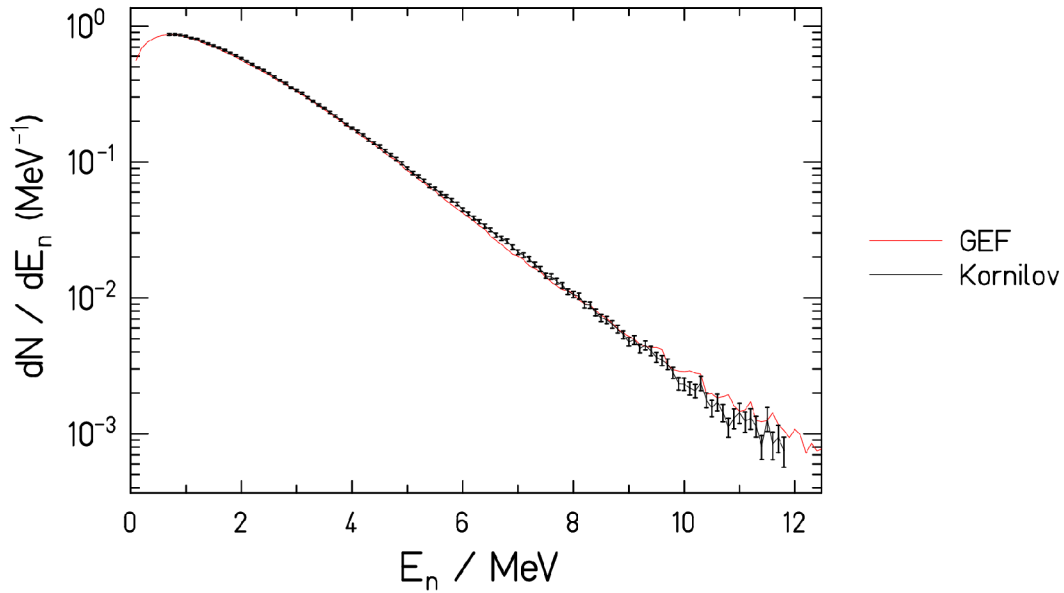


Figure 17. Experimental prompt-fission-neutron spectrum for ${}^{235}\text{U}(n_{\text{th}}, f)$ [¹⁰²] in comparison with the result of the GEF code.

$$\omega \propto \frac{\sqrt{\pi}}{12 \tilde{a}^{1/4} U^{5/4}} \exp(2\sqrt{\tilde{a}U})$$

with $U = E + E_{\text{cond}} + \delta U(1 - \exp(-\gamma E))$, $\gamma = 0.055$ and the asymptotic level-density parameter $\tilde{a} = 0.078A + 0.115A^{2/3}$. The shift parameter E_{cond} represents the pairing-condensation energy given by $E_{\text{cond}} = -2 \text{ MeV} - n\Delta_0$, $\Delta_0 = \frac{12}{\sqrt{A}}$ with $n = 0, 1, 2$ for odd-odd, odd- A and even-even nuclei, respectively. δU is the ground-state shell correction. A constant spin-cutoff parameter was used. The matching condition with the constant-temperature part determines the scaling factor for the Fermi-gas part. It is related with the collective enhancement of the level density. Again, a better agreement with the measured prompt-neutron spectrum was achieved by increasing the asymptotic level-density parameter by 10%.

The excellent reproduction of the measured neutron spectrum in the whole lower-energy part up to 5 MeV does not give any indication for neutron emission at scission [¹⁰³, ¹⁰⁴, ¹⁰⁵, ¹⁰⁶] or from the fragments before full acceleration [¹⁰⁷, ¹⁰⁸], although a definite conclusion is difficult due to the uncertainties in the level densities and in the optical-model parameters.

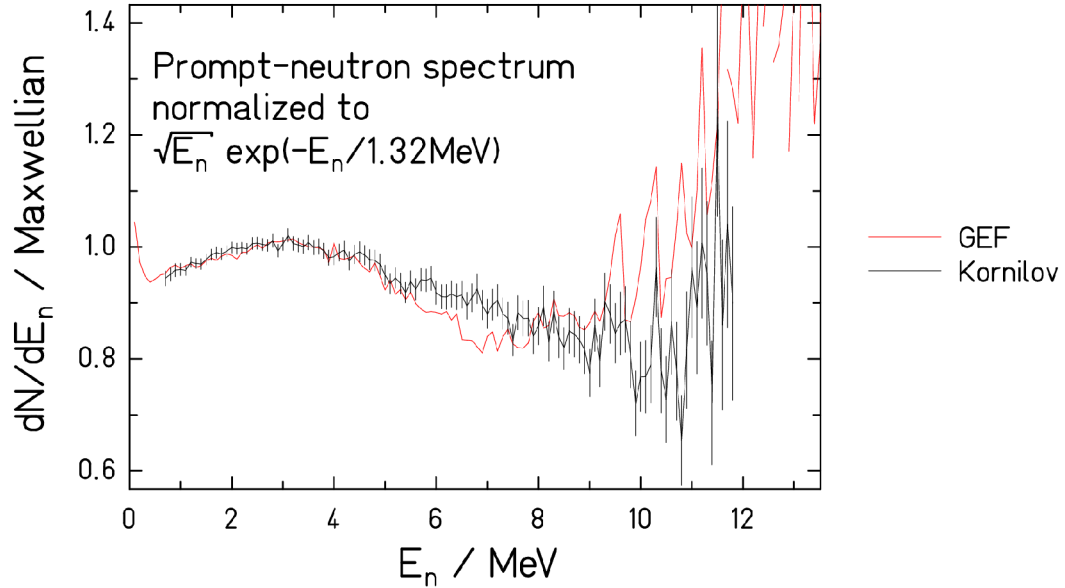


Figure 18. Experimental prompt-fission-neutron spectrum for $^{235}\text{U}(n_{\text{th}},f)$ [102] in comparison with the result of the GEF code. Both spectra have been normalized to a Maxwellian with $T = 1.32$ MeV.

Prompt-gamma emission

In figure 19, the calculated prompt-gamma spectrum for the system $^{235}\text{U}(n_{\text{th}},f)$ is compared with the experimental data of ref. [115]. One can distinguish the signatures of the different contributions to the gamma strength. The E1 emission from the GDR dominates the high-energy part above 2 MeV. E2 emission from rotational bands at the yrast line strongly fills up the spectrum below 2 MeV. The amount of E2 emission is constrained by the angular-momentum distribution of the fission fragments [109].

Detailed experiments with very high counting statistics and high-granularity detectors, e.g. with the Darmstadt-Heidelberg Crystal ball, have been performed for spontaneous fission of ^{252}Cf . These experiments cover an energy range up to 80 MeV including the whole GDR and extending to the postulated radiation from nucleus-nucleus coherent bremsstrahlung of the accelerating fission fragments [110], which is not considered in the GEF code. Several theoretical studies of the many complex features of these data have been performed, mostly with modified versions of the CASCADE code [111], see e.g. refs. [112, 113]. Figure 20 shows an overview on these data in comparison with the result of the GEF code up to 15 MeV. Obviously, the complex features of this spectrum are fairly well reproduced, in particular the kink near 8 MeV, approaching the peak energy of the GDR. The variation of the spectrum shape for different mass gates has been understood by the influence of shell effects, especially for nuclei near ^{132}Sn , on the de-excitation process [114].

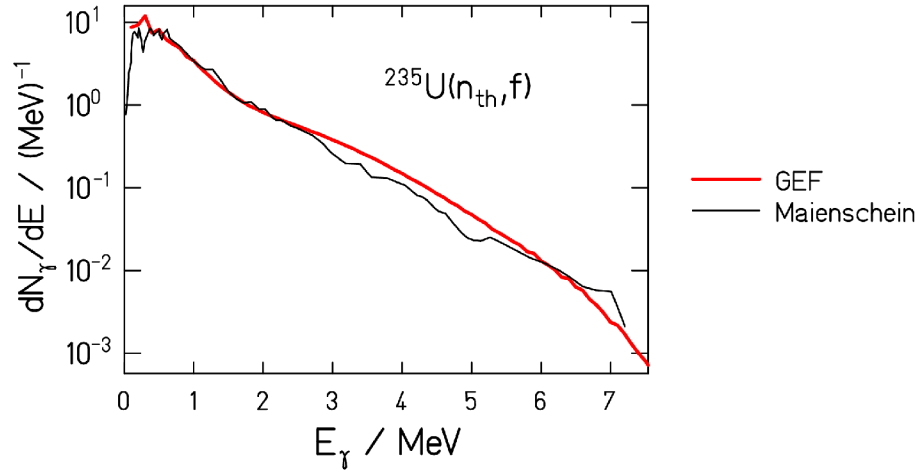


Figure 19. Experimental prompt-gamma spectrum for $^{235}\text{U}(n_{\text{th}}, f)$ [115] (thin black line) in comparison with the result of the GEF code (thick red line).

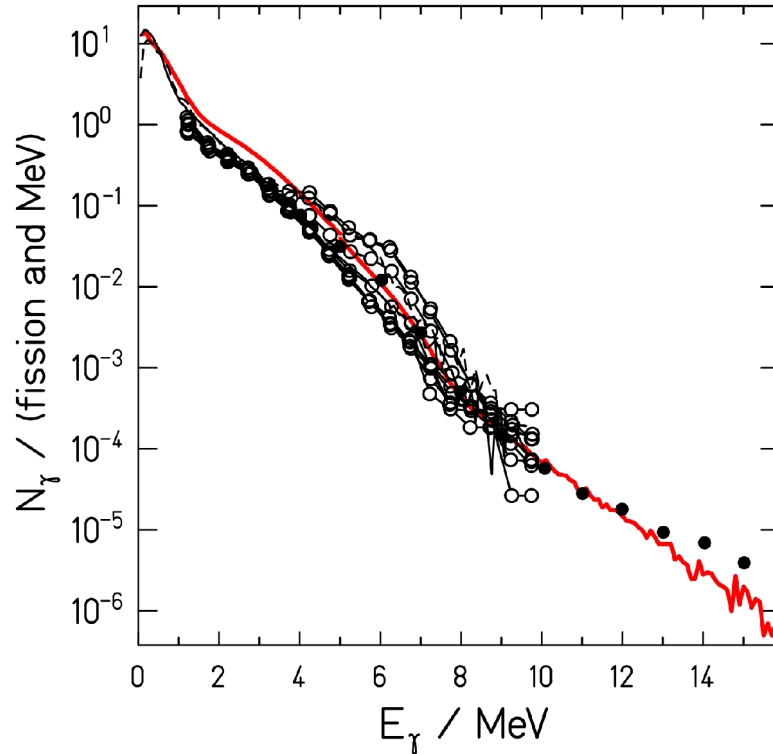


Figure 20. Experimental prompt-gamma spectrum for $^{252}\text{Cf}(sf)$ (data points and thin solid and dashed black lines) in comparison with the result of the GEF code (thick red line). Thin solid line: Raw spectrum from ref. [116], gate on the mass of the heavy fragment $126 \leq A_H \leq 136$. Thin dashed line: Raw spectrum from ref [116], gate on $144 \leq A_H \leq 154$. Open symbols: Deconvoluted spectra from ref. [117] with gates on different mass regions. Full symbols: Raw data from ref. [118].

X. SUMMARY

Due to the progress in experimental technology, the investigations of nuclear fission could considerably be extended to short-lived nuclei far from stability during the last 20 years, and data with better resolution could be obtained. Further advances are presently being made. This progress opened the view on several systematic trends not recognized before.

The previously claimed constant mean mass of the heavy component in asymmetric fission turned out to be biased by the restricted empirical knowledge. New data reveal that it is the position of the heavy component in Z , which is approximately constant. Theoretical arguments for this unexpected finding are not yet available.

For the even-odd effect in fission-fragment Z distributions, the general enhancement of light fission fragments with even number of protons has been established for all fissioning systems, also for those with an odd number of protons. Moreover, this enhancement was found to show a strong increase towards the most asymmetric mass splits.

The theoretical description of the fission process with microscopic models is still very difficult, since most advanced models in nuclear physics that have been developed for stationary states are not readily applicable to the decay of a meta-stable state. In addition, these models suffer from their tremendous demand on computing power, restricting severely the number of degrees of freedom to be investigated. Since quantum-mechanical effects are essential, stochastic approaches with classical models seem to be inadequate. Thus, the comprehensive description of the fission process with microscopic methods is a tremendous challenge for developments in physics and in computer technology. At present, microscopic theory is expected to strongly promote the understanding of specific features, but it is far from describing the fission process in its full complexity and its large number of observables.

In this situation, it is still promising to analyze the experimental findings by establishing systematic trends, by exploiting gross relations and by applying general laws of physics like the statistical model and thermodynamics. As an example, the semi-empirical fission model, implemented in the GEF code, reproduces a large variety of observables with a good precision in a consistent way without further adjustment to specific fissioning systems. With this global approach, one is able to predict several characteristic quantities of the fission process, e.g. the fission-fragment yields and the energy and multiplicity distribution of prompt-fission neutrons and gammas, without the need for specific experimental information of the respective system, e.g. measured mass-TKE distributions. All properties of the fission fragments that are considered in the code (e.g. nuclear charge, mass, excitation energy, angular momentum) are sampled in the corresponding multi-dimensional parameter space by a Monte-Carlo technique. Thus, all respective correlations are preserved. Moreover, correlations between all observables considered in the code are provided on an event-by-event basis. The good reproduction of

the manifold experimental data indicates a surprisingly high degree of inherent regularity and simplicity in the fission dynamics.

Probably the most important progress has been made by analyzing some complex features of prompt-neutron yields and even-odd effects in fission-fragment Z distributions with the methods of statistical mechanics. Evidence for energy sorting, a peculiar thermodynamical process in the pre-scission configuration, has been deduced from prompt-neutron yields. The threshold behaviour of the asymmetry-associated even-odd effect establishes a relation between the speed of the energy transfer between the nascent fragments and the dynamical time, starting at the moment when the two fragments develop their individual properties, e.g. their final temperatures, and the moment when the resistance against the transfer of protons across the neck becomes inhibitive. This new insight stresses the importance of nuclear fission as a laboratory for studying the dynamics of non-equilibrium processes in mesoscopic quantum-mechanical objects under the influence of residual interactions.

Acknowledgements

Part of this work has been supported by the NEA of the OECD (<http://www.oecd-nea.org/>), by the EFNUDAT (<http://www.efnudat.eu/>) and by the ERINDA (<http://www.erinda.org/>) projects of EURATOM.

APPENDIX

The appendix presents a comprehensive comparison of measured or evaluated fission-fragment mass and nuclear-charge distributions with the results of the GEF code in logarithmic and linear scale. In this way, the quality of the reproduction of the mass yields can be seen over the whole range of fissioning systems. All calculations have been performed with a unique set of model parameters.

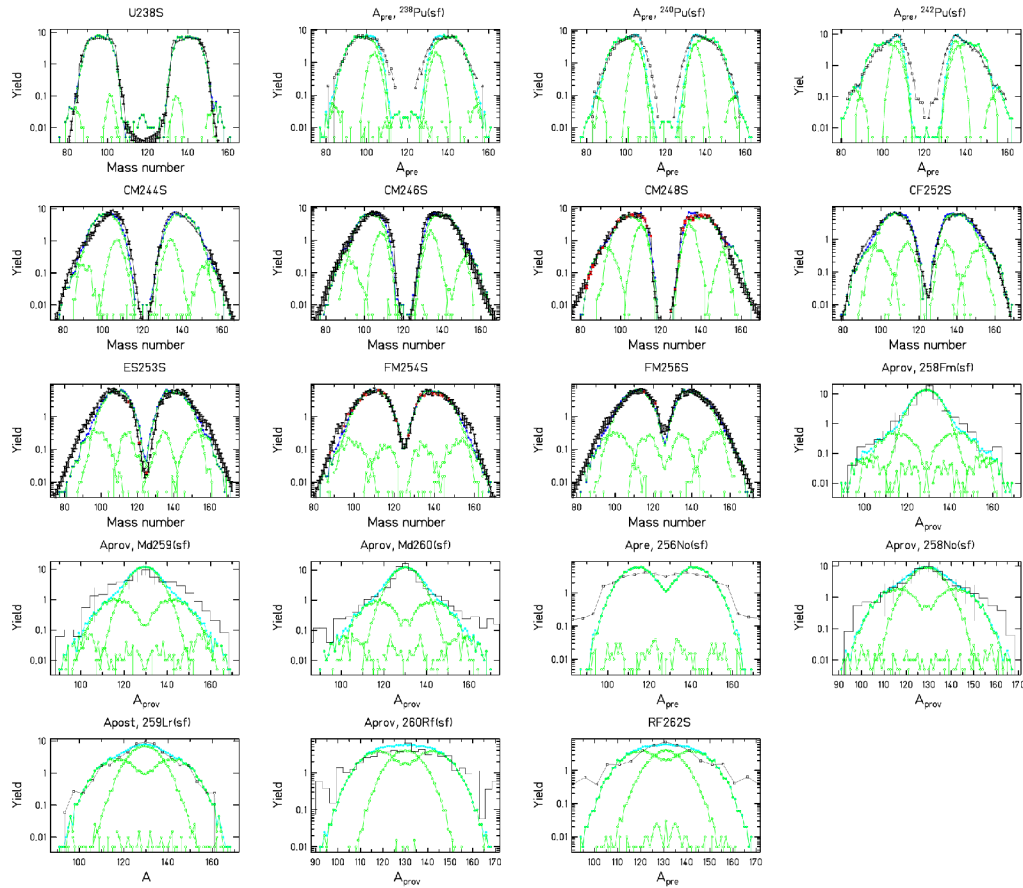


Figure A1. Mass and Z distributions of fission fragments from spontaneous fission. (In most cases the post-neutron masses are shown. A_{prov} is the “provisional mass” that is directly deduced from the ratio of the kinetic energies of the fragments and, thus, it is not corrected for neutron emission.) Measured or evaluated data (black lines, respectively histogram) are compared with predictions of the GEF code [29] (pink and green lines). The contributions of different fission channels are shown. (See [29] for references of the data.)

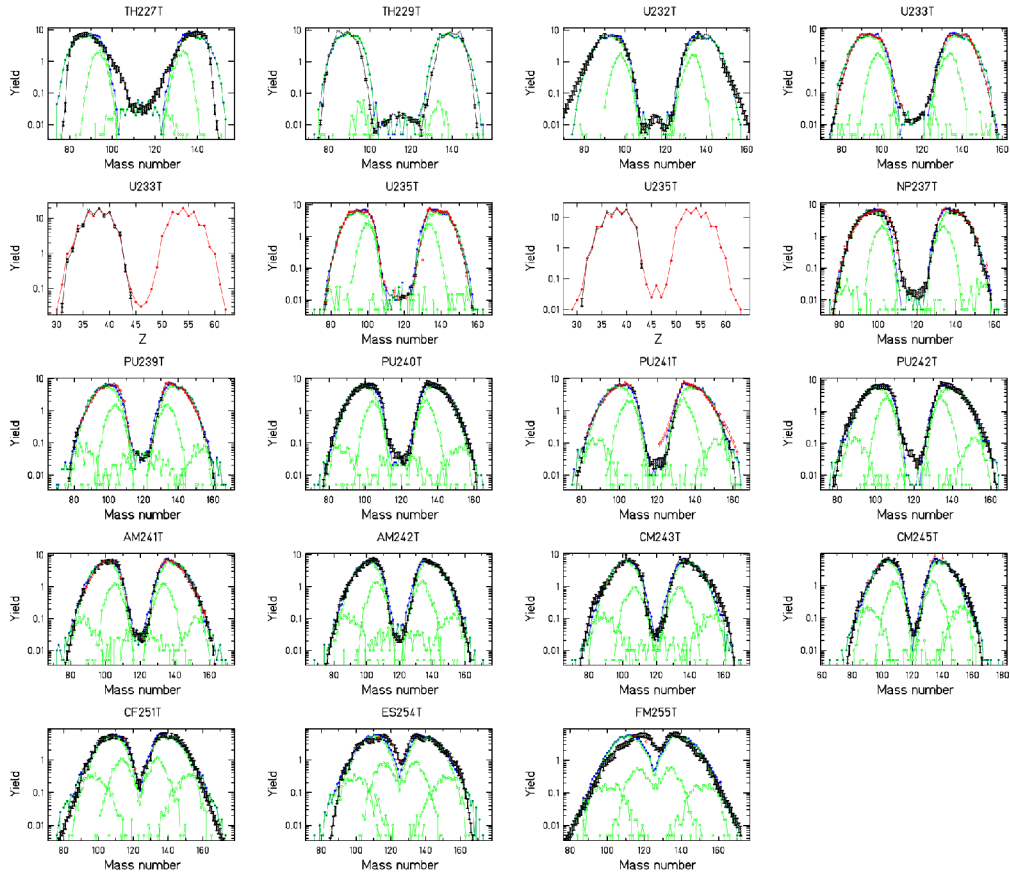


Figure A2. Nuclear-charge and mass distributions of fission fragments from thermal-neutron-induced fission. Measured or evaluated data (black lines, respectively histogram) are compared with predictions of the GEF code [29] (red and green lines). The contributions of different fission channels are shown. (See [29] for references of the data.)

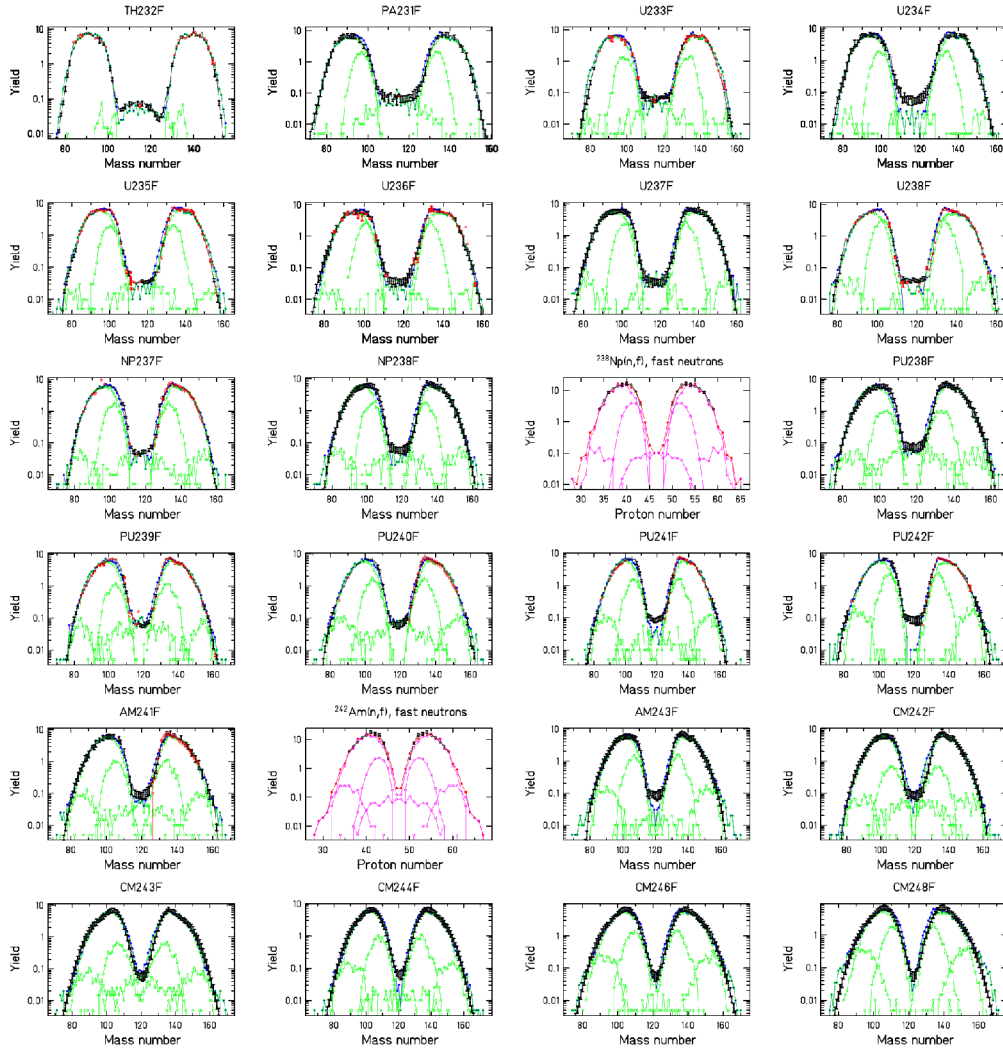


Figure A3. Nuclear-charge and mass distributions of fission fragments from fast-neutron-induced fission. Measured or evaluated data (black lines, respectively histogram) are compared with predictions of the GEF code [29] (red and green lines). The contributions of different fission channels are shown. (See [29] for references of the data.)

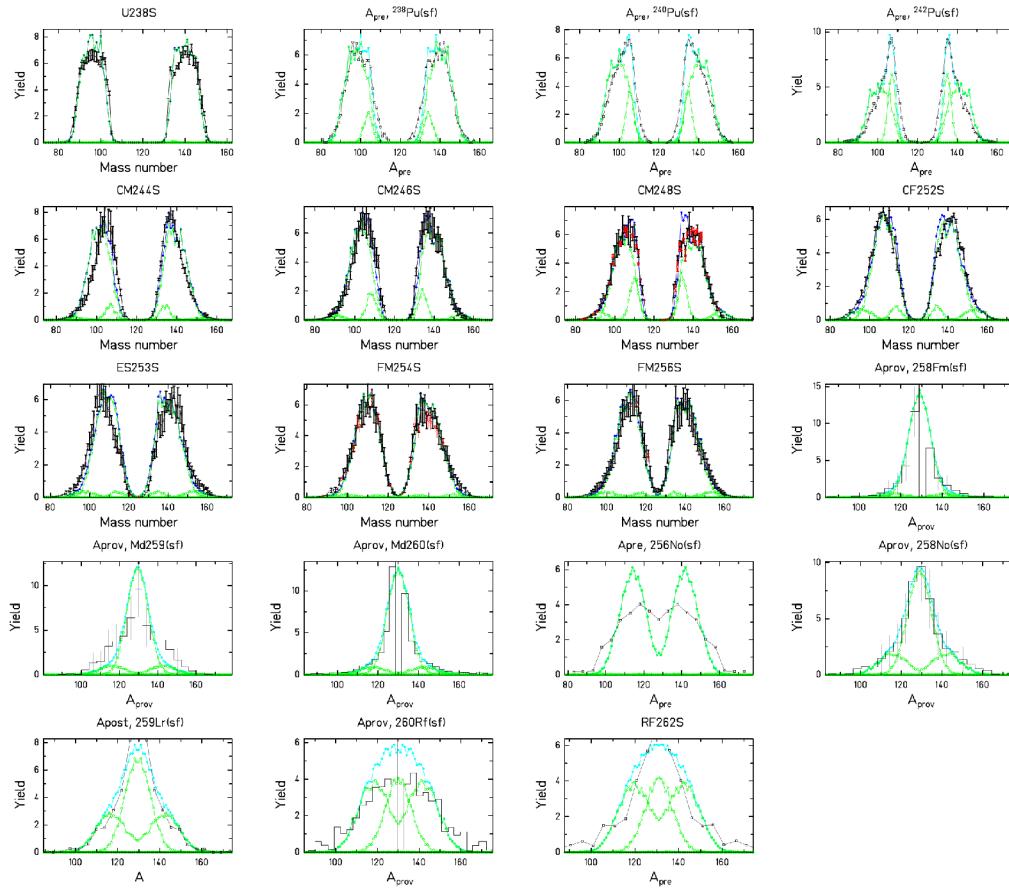


Figure A4. Like figure A1, but in linear scale.

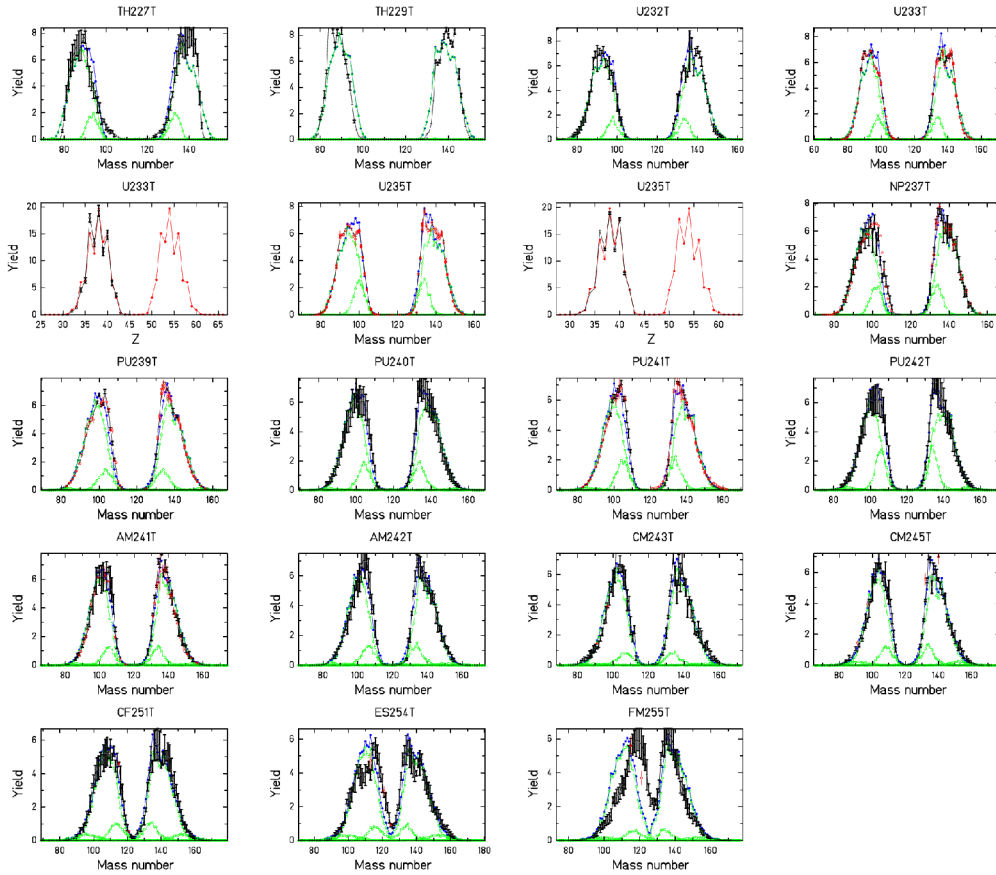


Figure A5. Like figure A2, but in linear scale.

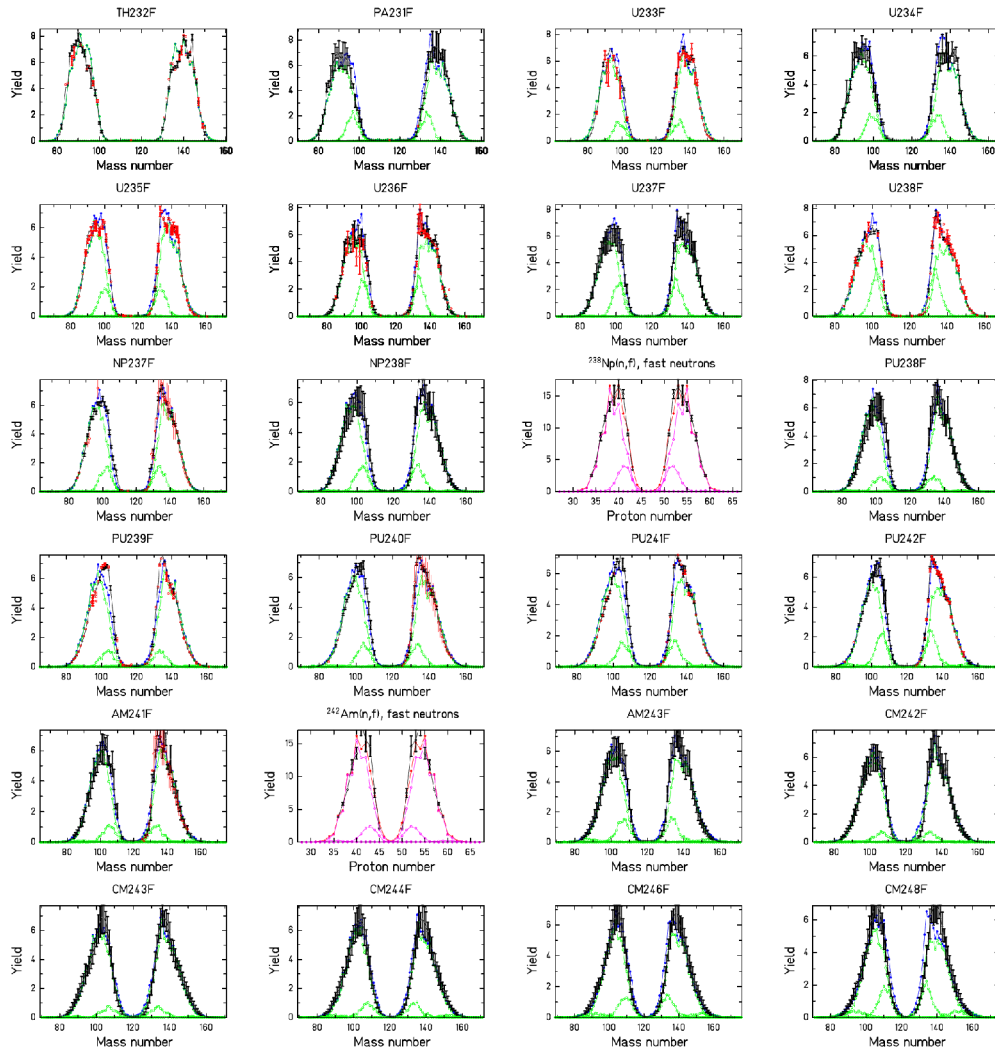


Figure A6. Like figure A3, but in linear scale.

- 1 Otto Hahn, Fritz Straßmann, *Naturwissenschaften* 27 (1939) 89.
- 2 N. Bohr, J. A. Wheeler, *Phys. Rev.* 56 (1939) 426.
- 3 M. Goeppert-Mayer, *Phys. Rev.* 74 (1948) 235.
- 4 O. Haxel, J. H. D. Jensen, H. E. Suess, *Phys. Rev.* 75 (1949) 1766.
- 5 S. G. Nilsson, *Kgl. Danske Videnskab. Selskab, Mat.-Fys. Medd.* 29 (1955) 16.
- 6 *Nuclear Fission Process*, C. Wagemans ed., CRC Press Inc., (1991).
- 7 U. Brosa, S. Grossmann, A. Müller, *Phys. Rep.* 197 (1990) 167.
- 8 H. Nifenecker et al., *Z. Phys. A* 308 (1982) 39.
- 9 J. P. Bocquet, R. Brissot, *Nucl. Phys. A* 502 (1989) 213c.
- 10 F.-K. Thielemann et al., *Int. J. Mod. Phys. E* 16 (2007) 114.
- 11 I. V. Panov et al., *Nucl. Phys. A* 747 (2005) 633.
- 12 J.-P. Delaroche et al., *Nucl. Phys. A* 771 (2006) 103.
- 13 D. Jacquet, M. Morjean, *Prog. Part. Nucl. Phys.* 63 (2009) 155.
- 14 K.-H. Schmidt, B. Jurado, *Phys. Rev. C* 82 (2011) 014607.
- 15 S. G. Kadmsky, *Phys. Atom. Nucl.* 70 (2007) 1628.
- 16 V. V. Pashkevich, *Nucl. Phys. A* 169 (1971) 275.
- 17 C. F. von Weizsäcker, *Z. Phys.* 96 (1935) 431.
- 18 P. Möller, D. G. Madland, A. J. Sierk, A. Iwamoto, *Nature* 409 (2001) 785.
- 19 T. Asano, T. Wada, M. Ohta, T. Ichikawa, S. Yamaji, H. Nakahara, *J. Nucl. Radioch. Sc.* 5 (2004) 1.
- 20 T. Asano, T. Wada, M. Ohta, S. Yamaji, H. Nakahara, *J. Nucl. Radioch. Sc.* 7 (2006) 7.
- 21 J. Randrup, P. Möller, A. J. Sierk, *Phys. Rev. C* 84 (2011) 034613.
- 22 P. Möller, J. Randrup, A. J. Sierk, *Phys. Rev. C* 85 (2012) 024306.
- 23 H. Goutte, J. F. Berger, P. Casoli, D. Gogny, *Phys. Rev. C* 71 (2005) 024316.
- 24 H. Goutte et al., *Intern. J. Mod. Phys. E* 15 (2006) 292.
- 25 J. Randrup, P. Möller, *Phys. Rev. Lett.* 106 (2011) 132503.
- 26 C. Böckstiegel et al., *Nucl. Phys. A* 802 (2008) 12.
- 27 M. Caamaño et al., *J. Phys. G: Nucl. Part. Phys.* 38 (2011) 035101.
- 28 K.-H. Schmidt et al., *Europh. Lett.* 83 (2008) 32001.
- 29 <http://www.cenbg.in2p3.fr/GEF>, <http://www.cenbg.in2p3.fr/GEFY>
- 30 A. Ghiorso, T. Sikkeland, M. J. Nurmi, *Phys. Rev. Lett.* 18 (1967) 401.
- 31 A. N. Andreyev et al., *Phys. Rev. Lett.* 105 (2010) 252502.
- 32 K.-H. Schmidt et al., *Nucl. Phys. A* 665 (2000) 221.
- 33 F. Farget, private communication (2011).
- 34 X. Derkx et al., *EPJ Web of Conferences* 2 (2010) 07001.
- 35 A. N. Antonov et al., *Nucl. Instrum. Meth. A* 637 (2011) 60.
- 36 E. A. C. Crough, *At. Data Nucl. Data Tables* 19 (1977) 419.
- 37 W. E. Stein, *Phys. Rev.* 108 (1957) 94.
- 38 J. C. D. Milton and J. S. Fraser, *Phys. Rev.* 111 (1958) 877.
- 39 H. W. Schmitt, W. E. Kiker, C. W. Williams, *Phys. Rev.* 137 (1965) B837.
- 40 E. Moll et al., *Nucl. Instrum. Methods* 123 (1975) 615.
- 41 C. Donzaud et al., *Eur. Phys. J. A* 1 (1998) 407.
- 42 U. L. Businaro, S. Gallone, *Nuovo Cimento* 1 (1957) 1277.
- 43 M. G. Itkis et al., *Phys. Atom. Nucl.* 58 (1995) 2026.
- 44 S. M. Polikanov, *Sov. Phys. USPEKHI* 15 (1973) 48.
- 45 B. D. Wilkins, E. P. Steinberg, R. R. Chasman, *Phys. Rev. C* 14 (1976) 1832.
- 46 M. G. Itkis et al., *Sov. J. Nucl. Phys.* 52 (1990) 601.
- 47 S. I. Mulgin, K.-H. Schmidt, A. Grewe, S. V. Zhdanov, *Nucl. Phys. A* 640 (1998) 375.

- 48 J. P. Unik et al., Proc. Symp. Phys. Chem. Fission, Rochester 1973, IAEA Vienna (1974), vol. 2, p. 19.
- 49 I. Ragnarsson, R. K. Sheline, Phys. Scr. 29 (1984) 385.
- 50 M. Brack et al., Rev. Mod. Phys. 44 (1972) 320.
- 51 U. Mosel, H. Schmitt, Phys. Rev. C 4 (1971) 2185.
- 52 K.-H. Schmidt, A. Kelic, M. V. Ricciardi, Europh. Lett. 83 (2008) 32001.
- 53 A. S. Jensen, T. Døssing, Proc. Symp. Phys. Chem. Fission, Rochester 1973, IAEA Vienna (1974), vol. 1, p. 40.
- 54 D. Bucurescu, T. von Egidy, Phys. Rev. C 72 (2005) 06730.
- 55 A. V. Voinov et al., Phys. Rev. C 79 (2009) 031301.
- 56 A. V. Karpov, P. N. Nadtochy, D. V. Vanin, G. D. Adeev, Phys. Rev. C 63 (2001) 054610.
- 57 A. Ya. Rusanov, M. G. Itkis, V. N. Oklovich, Phys. At. Nucl. 60 (1997) 683.
- 58 A. V. Karpov, G. D. Adeev, Eur. Phys. J. A 14 (2002) 169.
- 59 H. Nifenecker, J. Physique Lett. 41 (1980) 47.
- 60 B. Bouzid et al., J. Phys. G: Nucl. Part. Phys. 24 (1998) 1029.
- 61 J. R. Nix, Ann. Phys. 41 (1967) 52.
- 62 L. Bonneau, P. Quentin, I. N. Mikhailov, Phys. Rev. C 75 (2007) 064313.
- 63 F. Gönnerwein, I. Tsekhanovich, V. Rubchenya, Intern. J. Mod. Phys. E 16 (2007) 410.
- 64 S. G. Kadmsky, Phys. Atom. Nucl. 71 (2008) 1193.
- 65 L. G. Moretto, G. F. Peaslee, G. J. Wozniak, Nucl. Phys. A 502 (1989) 453c.
- 66 J. R. Nix, Nucl. Phys. A 130 (1969) 241.
- 67 V. M. Kolomietz, S. Åberg, S. V. Radionov, Phys. Rev. C 77 (2008) 014305.
- 68 W. J. Swiatecki, S. Bjørnholm, Phys. Rep. 4 (1972) 32.
- 69 N. Dubray, H. Goutte, J.-P. Delaroche, Phys. Rev. C 77 (2008) 014310.
- 70 A. A. Naqvi, F. Käppeler, F. Dickmann, R. Müller, Phys. Rev. C 34 (1986) 21.
- 71 E. Algin et al., Phys. Rev. C 78 (2008) 054321.
- 72 M. Guttormsen et al., Phys. Rev. C 68 (2003) 034311.
- 73 Y. Alhassid, G. F. Bertsch, L. Fang, Phys. Rev. C 68 (2003) 044322.
- 74 G. G. Dussel, S. Pittel, J. Dukelsky, P. Sarriguren, Phys. Rev. C 76 (2007) 011302.
- 75 K.-H. Schmidt, B. Jurado, Phys. Rev. Lett. 104 (2010) 21250.
- 76 K.-H. Schmidt, B. Jurado, Phys. Rev. C 83 (2011) 061601.
- 77 W. J. Swiatecki, Prog. Part. Nucl. Phys. 4 (1980) 383.
- 78 R. Müller, A. A. Naqvi, F. Käppeler, F. Dickmann, Phys. Rev. C 29 (1984) 885.
- 79 C. J. Bishop et al., Nucl. Phys. A 150 (1970) 12.
- 80 A. C. Wahl, Phys. Rev. C 32 (1985) 184.
- 81 B. L. Tracy et al., Phys. Rev. C 5 (1972) 222.
- 82 M. Caamaño, F. Rejmund, K.-H. Schmidt, J. Phys. G: Nucl. Part. Phys. 38 (2011) 035101.
- 83 F. Rejmund, A. V. Ignatyuk, A. R. Junghans, K.-H. Schmidt, Nucl. Phys. A 678 (2000) 215.
- 84 S. Steinhäuser et al., Nucl. Phys. A 634 (1998) 89.
- 85 K.-H. Schmidt, B. Jurado, arXiv:1007.0741v1[nucl-th] (2010).
- 86 W. Lang et al., Nucl. Phys. A 345 (1980) 34.
- 87 W. Nörenberg, Z. Phys. 197 (1966) 246.
- 88 K. T. R. Davies, A. J. Sierk, J. R. Nix, Phys. Rev. C 13 (1976) 2385.
- 89 M. Asghar, R. W. Hasse, J. Phys. Colloques 45 (1984) C6-455.
- 90 G. Schuette, L. Wilets, Nucl. Phys. A 252 (1975) 21.
- 91 D. G. Madland, R. J. LaBauve, J. R. Nix, IAEA-INDC(NDS)-220 (1989) 259.
- 92 A. Tudora et al., Nucl. Phys. A 756 (2005) 176.
- 93 A. Tudora, Ann. Nucl. Energy 33 (2006) 1030.
- 94 M. S. Zucker, N. E. Holden, Report BNL-38491 (1986).

- 95 E. J. Axton, Nucl. Stand. Ref. Data (1985) 214.
- 96 J. R. Huizenga, R. Vandenbosch, Phys. Rev. 120 (1960) 130.
- 97 A. J. Koning, J. P. Delaroche, Nucl. Phys. A 713 (2003) 231.
- 98 A. R. Junghans et al., Phys. Lett. B 670 (2008) 200.
- 99 T. von Egidy, D. Bucurescu, Phys. Rev. C 78 (2008) 05130.
- 100 A. V. Ignatyuk, G. N. Smirenkin, A. S. Tishin, Sov. J. Nucl. Phys. 21 (1975) 255.
- 101 A. V. Ignatyuk, Hadrons Nuclei Appl. 3 (2001) 287.
- 102 N. V. Kornilov et al., Nucl. Science Engin. 165 (2010) 117.
- 103 N. V. Kornilov et al., Nucl. Phys. A 686 (2001) 187.
- 104 G. V. Danilyan et al., Phys. Atom. Nucl. 71 (2008) 200.
- 105 G. A. Petrov et al., Phys. Atom. Nucl. 71 (2008) 1137.
- 106 N. Carjan. M. Rizea, Phys. Rev. C 82 (2010) 01461.
- 107 V. P. Eismont, Atomn. Ener. 19 (1965) 113.
- 108 V. M. Maslov et al., Eur. Phys. J. A 18 (2003) 93.
- 109 H. Naik, S. P. Dange, R. J. Singh, Phys. Rev. C 71 (2005) 014304.
- 110 S. P. Maydanyuk et al., Phys. Rev. C 82 (2010) 014602.
- 111 F. Pühlhofer, Nucl. Phys. 280 (1977) 267.
- 112 D. J. Hofman et al., Phys. Rev. C 47 (1993) 1103.
- 113 H. van der Ploeg et al., Nucl. Phys. A 569 (1994) 83.
- 114 H. von der Ploeg et al., Phys. Rev. C 52 (1995) 1915.
- 115 R. W. Pelle, F. C. Maienschein, Phys. Rev. C 3 (1971) 373.
- 116 P. Singer et al., Z. Phys. A 359 (1997) 41.
- 117 A. Hotzel et al., Z. Phys. A 356 (1996) 299.
- 118 D. Pandit et al., Phys. Lett. B 690 (2010) 473.